ISSN 0915-633X

NATIONAL INSTITUTE FOR FUSION SCIENCE

Study of Au^- Production in a Plasma-Sputter Type Negative Ion Source

Y. Okabe

(Received – Oct. 4, 1991)

NIFS-115 Oct. 1991

RESEARCH REPORT
NIFS Series

NAGOYA, JAPAN

Study of Au^- Production in a Plasma-Sputter Type Negative Ion Source

Yushirou OKABE

National Institute for Fusion Science
Nagoya 464-01

Dr. Sci. Thesis presented to

The Graduate School of Nagoya University

This work was performed under the Collaborating Research Program of the National Institute for Fusion Science, and was partly supported by the Grant-in-Aid for Scientific Research from the Ministry of Education, Science and Culture.

ABSTRACT

A negative ion source of plasma-sputter type has been constructed for the purpose of studying physical processes which take place in the ion source.

Negative ions of gold are produced on the gold target which is immersed in an argon discharge plasma and biased negatively with respect to the plasma. The work function of the target surface was lowered by the deposition of Cs on the target.

An *in-situ* method has been developed to determine the work function of the target surface in the ion source under discharge conditions by measuring the photoelectron currents induced by two lasers (He-Ne, Ar^+ laser) simultaneously injected onto the target. The reflectivity at each wavelength on a cesiated gold surface was measured and taken into account in deriving the work function from the photoelectron current measured.

The dependence of Au^- production rate, defined as the ratio of Au^- current to the target current, on the work function of the target surface was obtained from simultaneous measurements of both target surface work function and Au^- production rate while the Cs coverage was changed due to the plasma ion sputtering. The observed minimum work function of a cesiated gold surface in an argon plasma was

1.3 eV, when the negative ion production rate took the maximum value. The production rate increased monotonically and saturated when the surface work function was reduced from 1.9 eV to 1.3 eV. This range of the change in the work function was limited by the wave lengths of lasers used for the determination of the work function.

The dependence of Au^- production rate on the incident ion energy was deduced by changing the target bias voltage while the work function was kept constant. The production rate increased with the target bias voltage, and showed a similar dependence on the incident ion energy as the sputtering rate of gold with Ar^+ bombardment.

The dependence of Au^- production rate on the number of the incident ion was studied by changing the plasma discharge current, while the work function was again kept constant. The ion density increases linearly with the discharge current. Both negative ion current and target current increased linearly with discharge current, but the negative ion production rate remained constant in this range of discharge current.

From the experimental results, it is shown that the sputtering process is an important physical process for the negative ion production in the plasma-sputter type negative ion source.

The energy distribution function was also measured with an electrostatic energy analyzer. When the bias voltage was smaller than about 280 V, the high energy component in the distribution decreased as the target voltage was decreased. Therefore, the energy spread ΔE, which was defined as the full width at half maximum (FWHM) of

the observed negative ion energy distribution also decreased. This tendency is also seen in the energy spectrum of Cu atoms sputtered in normal direction by Ar^+ ions. The energy spread ΔE was between 4 and 10 eV when the target voltage was smaller than 300 V.

From the consideration of the negative ion production rate and the energy spread, the Au^- beam produced in the plasma-sputter type negative ion source is found applicable to the heavy ion beam probing (HIBP) which is a diagnostic technique for the plasma potential in a magnetically confined plasma.

KEYWORDS

Au^-, work function, plasma, negative ion source, photoelectric effect, negative ion beam, energy spread, electrostatic energy analyzer, heavy ion beam probe, plasma potential

Acknowledgements

I am greatly indebted to Professor Junji Fujita for his continual guidance, encouragement and helpful discussions during the course of this work.

For the most valuable discussions and the help in experiments, I do deeply thank Research Associate Mamiko Sasao. Also, I want to express my great appreciation to Associate Professor Motoi Wada in Doshisha University for his lectures on negative ion source, physics of negative ion formation and writing of scientific papers, Dr. Hitoshi Yamaoka for the construction of the plasma-sputter type Au^- ion source system and many effective suggestions.

Very helpful discussions with Dr. Yasunori Yamamura, Dr. Takaichi Kawamura and Dr. Hiroyuki Tawara about the sputtering phenomenon and atomic processes.

I much thank Dr. Shigeki Okajima, Dr. Isamu Ogawa, Dr. Ritoku Ando and Dr. Morihiko Sato for their useful suggestion and encouragement.

Finally, I do thank for many advices given by the people in the National Institute for Fusion Science and those in the Nagoya University.

Table of Contents

§1. Introduction

Plasma-sputter-type negative ion source is a kind of negative ion source and produces negative ions by the sputtering process. When the plasma ions sputter the metal surface which is immersed in a plasma and biased negatively with respect to the plasma, the sputtered target atom captures the electron if the target work function were low. The produced negative ions are accelerated to the plasma through the sheath. By the proper choice of the sputtering area and the shape of the target with respect to the plasma volume, heavy negative ions with a high current density can be obtained.

This type of negative ion source was recently developed by Alton *et al.*[1] and Mori *et al.*[2] Originally, this source was developed for the application to a beam source of the heavy ion beam accelerator, but now it is also used for the beam source of the ion implantation technic in the plasma processing. Another application as a beam source is considered. The relation of negative ion formation and physical parameters has not been precisely clarified yet since it was developed recently and the study to obtain a large current with a high current density has been performed.

Two physical parameters are considered to be dominant for the relation of the negative ion production in a plasma-sputter type

negative ion source. One is the reduction of the target work function, and the other is the sputtering yield that is a function of the target voltage. The negative ion production rate at the target surface is supposed to be larger when the work function of the surface is lower. Therefore, cesium is usually deposited onto the target surface in order to reduce the work function, and to increase the negative ion production rate.

An energetic particle impinging on a solid surface will share its kinetic energy with atoms in the solid via a series of collisions known as the collision cascade. If an atom near the solid surface receives enough energy from one of these collisions to overcome the surface binding energy, it could be ejected (or sputtered) into the vacuum. When the incident energy is below a few keV, the sputtering yield increases as the mass of the incident particle is heavier and the incident energy is higher. This results in a higher negative ion production rate at higher incident particle energy. However, the coverage of the alkali metal on the target will be also reduced by sputtering. This changes the target work function and the negative-ion formation. Thus, the negative ion production in an actual ion source is determined by the combination of the target work function and the target voltage which changes the incident ion energy. Mori *et al.* reported a higher production of Au^- compared with the other negative ions produced in the plasma-sputter-type negative ion source.[3] Sasao *et al.* reported that the cesiated gold target work function decreased

to about 1.5 eV.[4] However the work function dependence of Au^- production has not been precisely clarified yet. Therefore, a measurement of the target work function is indispensable for investigating the Au^- production characteristics.

The local potential in a plasma is one of the most fundamental parameters for the magnetic confinement of a plasma. Not only the plasma potential itself, but also the potential fluctuation is important to understand physical phenomena in a plasma such as instabilities and anomalous transports. But the measurement is not easy for a high temperature plasma when a Langmuir probe can not be used. A heavy ion beam probe (H. I. B. P)[5-9] has been developed as a method to measure the local potential as well as the fluctuations of the potential and the density in a high temperature plasma.

For large fusion devices such as the Large Helical Device (LHD), the injection beam energy more than 5 MeV is indispensable for a beam probing system because of the strong magnetic field to confine a plasma. Considering the high neutralization efficiency in this energy range, the possibility of a tandem acceleration, and the low acceleration potential of the source chamber, a beam probing system based on negative heavy ions is attractive. One of the most promising candidates is a negative gold ion beam. The production rate of Au^- by sputtering is high because of the relatively high sputtering yield and the large electron affinity (2.3 eV) of gold.[10] The Au^- beam can penetrate into the plasma even at a high magnetic field because of the heavy mass of gold. For the application to the plasma potential measurement,

a small energy spread of the beam is important as well as the high beam intensity. This is because the amplitude of the potential fluctuation, which is supposed to be around a few percent of the plasma potential, is to be measured with a high accuracy. To confirm the applicability of the Au^- beam as the probing beam ion for the local plasma potential in a plasma, we must measure the energy distribution of the Au^- beam.

The purposes of the thesis are to clarify the relations of negative ion formation and plasma parameters in the ion source by investigating the characteristics of the ion source and to investigate the applicability to the beam source of the plasma diagnostic technic.

The outline of the thesis is as follows:

(1) Construction of the plasma-sputter type negative ion source

The principle of the negative ion source was similar to the one made by Mori *et al*[2] at the National Laboratory for High Energy Physics (KEK). Here, the negative ion source is not developed for obtaining a higher negative ion current but for investigating the negative ion formation mechanism. The size of the ion source chamber was small (the volume of the chamber was about 1 *l*). The ion source is operated in steady state mode with the low discharge power of ~5 W and the target bias was less than 280 V with respect to the plasma.

(2) Development of an *in situ* method to measure the work function

A novel method to measure the work function of the target *in-situ*

was developed. Two laser beams with different wavelength (He-Ne; 632.8 nm, Ar^+ 488 nm) were used at the same time.[11] By using this method we can get the absolute value of the work function. This method will also be useful to control the target surface condition and maintain a high negative ion production. The principle and system of the work function measurement are described in chapter 2.

(3) Study of the relation of the negative ion formation and physical parameters of the ion source.

The relation between Au^- production and the work function was studied. The effects of discharge current and target voltage on Au^- production under a constant work function were studied. These experiments were performed with measuring the work function by using the above described method.

(4) Applicability of Au^- beam to H. I. B. P. method.

The energy distribution and the beam intensity of Au^- beam extracted from the negative ion source were measured.

In chapter 2, the fundamental process of negative ion formation by sputtering is described. Chapter 3 treats the experimental apparatus and procedure. In chapter 4, experimental results and discussion are presented. The summary is described in chapter 5.

§2. Relevant Physics

2-1. Sputtering process

(a) General description

Surfaces of solids erode under particle bombardment. Erosion rates are characterized primarily by the *sputtering yield* Y which is defined as the mean number of emitted atoms per incident particles. The sputtering yield depends in general on the type and the state of the bombarded material, in particular the detailed structure and the experimental geometry. Reliable experimental values of Y usually lie in the region of $10^{-5} \leq Y \leq 1$ atoms per incident particle.

(b) Linear collision cascade theory

Many scientists have investigated the sputtering processes theoretically. Sigmund proposed the linear collision cascade theory on the basis of many models and experimental results of sputtering events. The application of this theory is limited but this theory is regarded as the most improved one.[12] The concept of this theory is to simplify the collision condition on the target surface. Imagine a plane in an infinite medium, as shown in Fig. 1. The incident fast ion collides with this

surface at one point. In this point, the incident fast ion collides with a target atom elastically and impinges it from the ordinary lattice point. This impinged atoms (knock-on atom) collides with another target atom and moves it away. The knock on atoms are produced in this subsequent process, which is the "cascade" of the knock on atom. The density of these atoms is considered to be negligibly low to make a collision of knock-on atom to knock-on atom, which is the meaning of "linear". Besides, knock-on atoms are produced at a constant rate in time and the target condition is in a "steady" state from the macroscopic view after the long time has passed. If an atom near the solid surface receives enough energy from one of these collisions to overcome the surface binding energy, it could be ejected (or sputtered) into the vacuum.

2-2. Negative ion formation process

To form an Au^- by sputtering, a gold atom must capture an electron from the Cs deposited on the surface or the target surface before it passes through the Cs layer. After the electron capture, the Au^- must leave the cesiated surface without transferring the electron back to the cesiated metal surface. The negative ion formation probability is considered to depend on both the work function of the metal surface and the velocity that the sputtered atom leaves from the surface.

(a) Work function dependence

As shown in Fig. 2, the energy difference E_A between the normal state of an atom and ion is called the electron affinity of the atom. This energy will also be equal to that necessary to detach an electron from the ion, so may also be called the electron detachment energy of the ion. A positive electron affinity indicates a stable negative ion. The higher electron affinity leads a stable condition of the negative ion. This is one of the most important parameters forming negative ions.

Consider the sputtered atom is in the vicinity of the metal surface. It weakly interacts with the metal, and electrons can tunnel between the atom and the solid. As is illustrated in Fig. 2, this process will shift

and broaden the electron affinity states to be a narrow band. The tail of this state may overlap the Fermi level of the metal, and the tunneling of an electron from the metal to the atom becomes possible. When the work function of the metal is lower than the electron affinity of the atom, an electron in the conduction band can be transferred to the atom in the vicinity of the metal surface. For the case of gold atom, the electron affinity is 2.3 eV but work function is 5.2~5.4 eV. However, if the alkali metal (Cs etc.) is adsorbed on the metal surface, then Cs releases an electron to the target surface because of its low ionized voltage. The work function of the target surface decreases with the electric dipole as the thickness of the alkali metal increases to some degree.[13] This process makes the gold atoms to capture electrons.

Imagine that a negative ion leaves the cesiated target surface of which the work function is higher than the electron affinity of the atom. We define X_0 as the distance at which the electron affinity of the atom becomes equal to the work function. In the region of $X < X_0$, negative ions are produced by the electron transfer from the Fermi level to the electron affinity of the atom. When the negative ion is in the region of $X > X_0$, some of the produced negative ions are neutralized by electron transfer back to the surface.

The faster the negative ion leaves the target surface, the smaller the probability to transfer the electron to the target surface. Therefore, the negative ion can survive more as the escaping velocity becomes faster. Considering the above mechanisms, when $\phi \leq E_a$, the negative ion formation probability β^- is given by[14)]

$$\beta^- = 1 - \frac{2}{\pi} \exp[-\pi \frac{e}{h}(E_a - \phi)/2Av_\perp], \quad (1)$$

where e is the unit charge of an electron, ϕ is the work function, E_a is the electron affinity of the negative ion, $v_\perp$ the velocity component of the negative ion normal to the surface, and A is a constant.

M. L. Yu showed experimentally that the work function dependence of negative ions, Mo^-, O^-, H^- and D^- produced by sputtering process.[15)] He revealed a possible tunneling mechanism from the fact that correlation with the work function changed when the surface electronic state was modified by a Cs overlayer.

The electron tunneling model proposed by Yu predicted the relation of the negative ion yield to the work function.[15)] The equation is given as below:

$$Y = AY_0 \frac{16E(V_1 + \Delta\varphi)}{V_0^2} \exp[-2(\frac{2m}{\hbar^2})^{\frac{1}{2}}(V_1 + \Delta\varphi)^{\frac{1}{2}} b] \quad (2)$$

where A is the neutralization probability of the ion, Y_0 is the total

sputtering yield, E is the energy of the electron, V_0 is the height of the tunneling barrier, V_1 is the initial barrier of the potential when there is no Cs, $\Delta\varphi$ is the work function change, and b is the potential width.

(b) Dependence upon the escaping velocity

The negative ion formation probability depends on the velocity that the atoms leave from the surface (escaping velocity). As the escaping velocity becomes faster, the electron transfer from the escaping atom to the target surface becomes more difficult. Therefore, the negative ion formation probability can be considered to increase as the escaping velocity becomes faster.

M. L. Yu also experimentally observed that the velocity dependence of the negative ion formation probability of sputtered O^- from chemisorbed oxygen layers on V and Nb.[16] He found that the negative ion formation probability depended on the normal component of the emission velocity $v_\perp$, which suggested that the ionization process was an ion-surface interaction and not an ion-atom binary interaction. For $v_\perp > 1 \times 10^6$ cm/sec, the ionization probability showed an exponential dependence on $v_\perp$. However, this velocity dependence failed at lower velocities. A thorough theoretical treatment still does not appear because of the apparent lack of experimental data on energy spectra.

The precise negative ion formation theory that describes the region where the work function is lower than the electron affinity has not

been presented yet. However, in this region the atom which captured electron is expected not to transfer it to the metal and the escaping energy dependence seems to be weak because of the higher energy difference between the work function and the electron affinity of the gold atom.

2-3. Principle of the work function measurement

An *in situ* method to measure the work function of the metal surface in a plasma was developed to obtain the correlation of absolute value of the target work function and the negative ion formation rate. In this method the work function was determined by measuring the photoelectric current induced by two lasers (He-Ne, Ar^+ laser) simultaneously. The difference of the absorptivity of two lasers were corrected by measuring the reflectivities of these two lights, respectively.

As an example of a change in the work function due to alkali metal coverage, that of the Cs-Mo surface as a function of Cs thickness is quoted from a Ph. D thesis by Wada and is shown in Fig. 3.[13] The work function of a bare Mo surface is 4.2 eV. By Cs adsorption, the work function falls from 4.2 eV to a minimum value of about 1.8 eV, and then increases again to 2.1 eV with increasing Cs thickness. Near the work function minimum, the probability of forming negative ions is maximized. In the case of gold, the work function of a bare surface is 5.3 ~ 5.5 eV.[10] It is expected that the change in the work function for the Cs-Au system has the same tendency as that for the Cs-Mo system.

The basic theory of photoelectron emission for clean metals at various temperatures was studied by Fowler.[17] When the energy of

an incident photon is close to the work function of a surface, the photon is absorbed by an electron near the surface and then the electron escapes from the metal with a kinetic energy corresponding to the difference between the potential energy and the incident photon energy. Here, the quantum efficiency Y is defined as the number of emitted electrons divided by the number of absorbed photons.

$$Y=\frac{(\ photoelectron\ \ number\ )}{(absorbed\ \ \ photon\ number\ )}. \tag{3}$$

Electrons in the conduction band of the metal follows Fermi-Dirac statistics, and the number of electrons per unit volume n is given by the following formula:[17)]

$$n=\frac{4\sqrt{2}\,\pi\, m^{\frac{3}{2}}\, k^2 T^2\, a}{h^3}\int_0^{\infty}\frac{\log\{1+\exp[-y+(h\nu-\Phi_w)/kT]\}}{\sqrt{y+(U_0-h\nu)/kT}}\,dy, \tag{4}$$

where m is the electron mass, U_o is the potential step at the boundary, $h\nu$ is the incident photon energy, Φ_w is the work function, and a is the absorptivity at the surface. In principle, the work function can be obtained by measuring the quantum efficiency of monochromatic light if U_o, a and T are known. However, in practice, it is not easy to measure the surface condition which changes drastically in a plasma.

The logarithm is expanded and integrated term by term with the limit of $T \rightarrow 0$, and the first term gives the following formula for the quantum efficiency:

$$Y \propto \frac{a(h\nu - \Phi_w)^2}{(U_0 - h\nu)^{\frac{1}{2}}}, \qquad h\nu > \Phi_w,$$
$$Y = 0, \qquad h\nu < \Phi_w. \tag{5}$$

If we assume a to be nearly constant, the square root of the quantum efficiency has an almost linear relationship with the work function. Here we must note that the theory is not a good approximation at a higher value of μ, where $\mu = (h\nu - \Phi_w)/kT$. However, if the surface temperature is not too high compared with the room temperature, we can use the approximate formula (5) to determine the work function. For a wider range of incident photon energy, eq. (4) is more accurate. In eq. (5), Y does not depend on its denominator because the value of U_o is normally large (11 ~ 20 eV) compared with $h\nu$; therefore, Y depends strongly on the numerator.

When monochromatic light from a laser is incident on the Cs-Au target surface, and if the work function is lower than the incident photon energy, the observed photoelectric current signal from the surface is a function of the work function. By using two different wavelength lasers simultaneously, two different photoelectric currents are obtained. The absolute value of the work function of a surface is calculated by the ratio of the value of these photoelectric currents:

$$\Phi_w = \frac{h\nu_1 - \zeta h\nu_2}{1-\zeta}, \qquad \zeta = \sqrt{\frac{(1-R_2)Y_1}{(1-R_1)Y_2}}. \tag{6}$$

Here, Y_1 and Y_2 are assumed proportional to the corresponding photoelectric current, and R_1 and R_2 ($R = 1 - a$) are reflectivities at each wavelength. The work function can be obtained by using relation (6) if the relative values of the quantum efficiencies and absorptivity at the two photon energies are measured.

§3. Experimental

3-1. Ion source

A schematic diagram of the experimental setup is shown in Fig. 4. From the view of the historical success of negative ion extraction, the shape of the ion source was a column which had been called "bucket type" ion source. For the good confinement of the plasma, the extraction port of this ion source is at the side of the column. The plasma is confined in the place where the magnetic field is weak. At the center of the plasma, there is a target to form negative ions by sputtering process. The mass of the extracted negative ions are so *heavy* that the pass of the beam is not affected by the magnetic field at the extraction port.

To make the cesium consumption less and the electric power to be used smaller, an ion source of which chamber volume is small is appropriate. The bigger size of the chamber has advantages because of its spatial capacity in observing the physical fundamental processes and for making the uniformity of the plasma to sputter the target surface. Considering these factors, the volume of the ion source was determined to be about 1 *l* which is smaller than that of the plasma-

sputter type negative ion source used in K. E. K. (nickname of the source is BLAKE) of about 6 *l*.

In order to investigate the negative ion formation procedure and monitor various parameters of the target, many ports, of reasonably big size were needed.

The ion source consisting of a chamber of 10.8 cm in diameter and 12 cm long stainless steel vessel, had six ports on its side and two ones on each end flange. The ion source was surrounded by eight columns of samarium cobalt magnets ($7 \times 7 \times 39$ mm) to form a multiline magnetic cusp geometry for the plasma confinement. By the spatial restriction, the number and the width of the magnet can be determined with the following relation.

$$\frac{\pi d}{n} > 18 + W > \frac{\pi d}{n+1} \tag{7}$$

Here, d is the diameter of the ion source, n is the number of the magnet and W is the width of the magnet. The number 18 (mm) came from the outer diameter of the observation port. The outer diameter of the negative ion extraction port was 38 mm which was the maximum value determined from the above formula. The inner diameter of this port was 34 mm by making the thickness of the wall of the port as thin as possible not to be bent by the ion source weight. The spatial profile of the magnetic field of the vacuum chamber is shown in Fig. 5. The magnet was assembled to three series and

placed in a water cooled manifold that touched the source chamber wall with a small contact area. Two ports on the side, were assembled so as to direct the target at 45 degree, for the laser beam injection and for observation of the reflected light. Because of the cesium oven installation, the port for the oven was rotatable flange. By flowing the warm water through these manifolds, the chamber wall was kept to be a constant temperature to avoid the cesium deposition. Each flange also had a water cooling system of which a copper pipe (ϕ 6 mm) was welded circularly around the magnets.

A steady-state plasma was generated by primary electrons emitted from a 0.05 cm diameter 8 cm long spiral shaped tungsten filament which was introduced from the side flange. The entire chamber wall served as an anode for the discharge. The filament was set in the field free region to prevent primary electrons from being captured by the magnetic field. The filament was biased 45 V negative with respect to the chamber when the discharge was performed. To avoid the multiple charged ions, the discharge voltage was maintained 45 V. When the filament voltage was about 8 V, the plasma was produced.

The inert gas such as Ar was introduced into the chamber through a needle valve (Type LB2B VALVE made in Edwards High Vacuum Co. Ltd). In this experiment, only argon gas was used because of the comparison of other experimental results of argon sputtering. The stop valve was used to decrease the flow rate through the needle valve and to make the control of the amount of flowing by the needle valve. These valves were connected with the synflex tubes. Argon gas was

filled in the gas introduction tube not to introduce the impurity components into the chamber after the tube was evacuated less than 10^{-5} Torr. When the pressure of the Ar reached about 1 mTorr, an argon arc plasma was produced.

A gold plate of 0.5 mm thick and 2.3 cm in diameter was attached to a water-cooled Cu target by electron-beam welding, and was used as the sputter target (sputter probe) of the ion source. The target to be sputtered was a 99.999 % pure gold plate. A schematic diagram of the target is shown in Fig. 6. The target was mounted inside of the chamber with a quartz glass shield to reduce the surface area exposed to the plasma.

By biasing the target negatively with respect to the plasma, positive ions from the plasma were accelerated across the sheath and struck the target surface. Negative ions of Au formed at the target surface were then accelerated back from the surface and measured by the beam diagnostic systems.

A cesium oven was used to deposit cesium vapor on the target. The structure of the oven is shown in Fig. 7. Originally the oven was installed at the side port directing the target at 45 °. Cesium deposited heavily near the exit of the port and inhomogeneously on the target. For the laser power absorptivity measurement, 45 ° port had to be used for the reflected laser power measurement. Therefore, the oven was moved to the side flange. Then the cesium was deposited uniformly on the target. The oven was wound by a heater wire

uniformly and covered with pieces of asbestos mats. The cesium oven temperature was measured by the thermocouple which was attached to the bottom of the valve. It was difficult to keep the uniform cesium deposition on the target because the cesium flow was changed sensitively by the oven temperature, the valve opening area, the residual cesium quantity, and the time after cesium was loaded in the oven, namely the oxidation of the cesium. The surface of cesium in the oven was oxidized to some extent during the loading procedure. To break the oxidized surface, oven was firstly heated to more than 300 °C with the valve tightly closed so as not to be loosened with thermal expansion. Secondly, the heating was stopped and the valve was opened after it was cooled down. When the temperature was decreased to about 120 °C, the oven was heated again to keep the temperature constant (130 °C). The cesium was also deposited to the chamber wall. By the plasma sputtering and the heating of the wall, cesium came off from the wall and a part of them deposited to the target surface. The target surface was water cooled to about 20 °C to enhance the cesium deposition. In order to control the cesium recycling from the wall, the chamber wall temperature was kept at around 60 °C with the hot water flow. Cesium deposited at the target surface was sputtered out by the plasma ions if the target were negatively biased.

The ion source was evacuated by a turbomolecular pump Osaka Vacuum TH-520 520 *l*/s through a 10 *l*/s pumping impedance

obtained with the measurement, and by an auxiliary rotary pump to the base pressure of less than 2.8×10^{-6} Torr. The valve (VAT) was mounted between the T. M. P. and detection chamber.

3-2. Work function measurement system

In order to measure the work function of a cesiated target (gold in this case) in a plasma, two laser beams modulated to different frequencies were injected onto the target simultaneously and the induced photoelectric currents were detected with two phase-sensitive detection system tuned at each frequency. One was an Ar^+ laser (Coherent Innova 100) which oscillated at several wave lengths, mainly 514.5 nm (2.41 eV) and 488 nm (2.54 eV), and had a total output power of about 1 W. The other was a He-Ne laser (NEC GLG5800) which had a wavelength of 632.8 nm (1.96 eV), and an output power of 50 mW. Each laser beam which passed through the chopper system was collimated and transmitted by the optical fiber. The beam from the fiber was reflected by two mirrors and injected into the chamber through the quartz glass. When the cesium was deposited on the glass, the transmissivity of the laser power was decreased. To keep the glass clean, the view port was heated with a wire heater (~100 °C). Considering the melting point of the viton O-ring (~150 °C), higher heating would cause the leakage. Before the ion source operation, each laser power was measured on the target by a power meter calibrated at each wavelength. The power of the Ar^+ laser measured on the target was 29.3 mW and that of the He-Ne

laser was 1.67 mW.

These laser beams were modulated by mechanical choppers to 263 Hz for the Ar^+ laser and 714 Hz for the He-Ne laser. The stainless steel disk plate chopper had 24 holes of 2 cm diameter. The thickness and the diameter of the chopper was 1mm and 24 cm, respectively. The chopper was attached to the variable motor (ORIENTAL MOTOR 51K 60FRA-A2) which equipped the speed (frequency) control system. The frequency can be modulated up to about 1000 Hz. The stainless steel chopper was painted to black so as to reduce the diffuse reflection of the beam. The velocity-variable motor was assembled on the heavy stainless steel dead weight to fix the chopper systems.

These lasers were mixed into one beam, and collimated on the same spot at the center of the target. The spot size was 1 cm in diameter on the target. The maximum output power of the He-Ne laser was smaller than that of the Ar^+ laser. Therefore the angles of two mirrors for guiding laser lights on the target were determined to make the He-Ne laser power monitored at the target maximum with the beam spot position and shape above mentioned.

During an operation of the source, the target was usually biased at V_t = - 100 ~ - 300 V, typically at - 200 V, and the typical target current was around I_t = 1 ~ 2 mA. Photoelectric currents induced by these two laser beams were less than 10^{-4} times the target current. The phase-sensitive method made the detection of the photoelectric current

possible at a high S / N ratio. The induced photoelectric current was doubled with the insulated transformer and separated from the plasma noise by using two lock-in amplifiers tuned at the frequency of each laser beam, and the outputs are connected to a multiparameter recorder system (GRAPHTECH MH9100). Most of electric signals of this system were transferred by coaxial-cables. The lock-in amplifier for the photoelectron induced by the He-Ne laser was of LI-575 NF Circuit Design Block Co. Ltd. and that by the Ar^+ laser was EG&G model 5210. A small portion of each laser beam modulated by each chopper system was detected by photo transistors, and amplified was used as the external reference signal of the lock-in amplifier.

A small portion of each laser beam is reflected by a optical glass before it passes the chopper system in order to monitor the injected power. The measured powers are recorded on the multiparameter recorder, as well as other ion source variables, the discharge current and the target current. The recorder can monitor 30 variables at the same time.

3-3. Au^- detection system

All species of singly charged negative ions produced in a plasma-sputter-type negative ion source have an initial energy nearly equal to the energy corresponding to the target voltage. Molecular ions broke up passing through plasma or on the way to the detection system. Masses of negative ion species from the source can be analyzed by a magnetic momentum analyzer (M. A.) located downstream of the beam. The cross sectional view of the mass spectrometer is shown in Fig. 8. Negative ions, after passing through the entrance slit (1 mm wide, 10 mm high), entered into a stainless steel case. They were deflected by the magnetic field and were collected at the faraday cups. Negative ions with low mass such as H^- are deflected 180 ° and that with high mass such as Au^-; $M/M_p = 197$, here, M is the mass of ion to be deflected and M_p is the mass of H^-, are slightly deflected to the opposite side of the 180 ° deflection by an opposite electromagnetic field. This magnet was driven by scanning the voltage. The voltage was controlled by a microcomputer (NEC PC-9801 VX) through a D-A converter (KIKUSUI GP-IB DPO2212A). The Faraday cup signal was shown on the display of the computer for confirming the Au^- production and then stored in the memory for data analysis. Faraday cup was made of brass coated with carbon to suppress the secondary electron emission. This cup was installed in the case made of Delrin.

The diameter of the entrance aperture of this cup is 0.5 mm width and 10 mm high. The aperture was also coated with carbon.

Without cesium introduction, the beam was dominated by impurity components. The negative impurities O^- ($M/M_p = 16$), $C_2H_2^-$ ($M/M_p = 26$) which was considered to come out from acetone (CH_3COCH_3; $M/M_p = 58$) or ethanol (C_2H_5OH; $M/M_p = 46$). Once the introduction of cesium vapor started, they disappeared and a peak corresponding to Au^- appeared. The following experiment was performed after confirming that the amount of impurity negative ion current is negligible compared to the Au^- ion current on the faraday cup for high mass analysis.

Then a movable Faraday cup (F. C.) at the upstream was introduced to the beam line and the vertical profile of the beam and time-dependent correlation to photoelectric currents were measured. Figure. 9 shows the cross-sectional view of the F. C. In the shield box of the movable F. C., a pair of permanent magnets were installed as well as an electron dump of graphite. A negative ion beam collimated by the entrance aperture of 3 mm diameter passed through the magnetic field, but electrons were suppressed by the magnetic field. Therefore, only negative ions were detected by the F. C. Another weak magnetic field was also applied to suppress the secondary electrons from the faraday cup. The details of the F. C. system were described in ref. 18. The detected current of Au^- was also recorded on the multiparameter recorder.

The retarding potential-type electrostatic analyzer (E. S. A.) which moved in the direction perpendicular to the Au^- ion beam was used for the measurement of the energy spread of a negative ion beam. A schematic diagram of the E. S. A. is shown in Fig. 10. Negative ions which passed through three Mo mesh grids were collected by 10 mm diameter disc collector made of brass coated with carbon. The diameter of the Mo wire is 0.03 mm and these wires consist 100 meshes per one inch. The transmissivity of these three mesh grids were 96 %. The scattering of the beam by these mesh grids were negligible. Negative ions were repelled by grid G_2 which was biased negatively with respect to the collector case. The energy spread of the beam was obtained from the signal detected by scanning the bias voltage from V_t + 30 to V_t - 30 volts. The bias voltage to the grid G_2 was scanned with 512 steps by a micro computer through the A-D converter above mentioned. The collector current was digitized by a digital electrometer (ADVANTEST R8340) and stored in the memory of the micro computer for data analysis. Because of the spatial restriction, F. C. and E. S. A. were not used at the same time.

3-4. Experimental procedure

To insure a consistent operation of the ion source, the following procedure were taken before each experimental measurement.

(1) Cleaning the ion source

(2) Cs loading

(3) Set up of the work function measurement system

(4) Start-up of the ion source

In some case that the residual cesium was enough, only step 4 was taken.

(a) Cleaning of the Ion source

Cesium inside of the ion source chamber absorbed by or reacted with residual impurity gases and accumulated them in the source, especially when the source chamber was opened up to atmosphere. Cesium inside the chamber deposited on the wall and the target surface. When the amount of the introduced cesium was too much to be sputtered out from the target surface, Au^- was not formed by the masking of the gold surface due to Cs. Moreover, the port for the laser beam injection was covered with Cs and / or sputter Au and photoelectron current was not detected. When too much Cs was accumulated in the chamber, it had to be cleaned. Before opening the chamber, Ar gas was introduced into the chamber to suppress

accumulated Cs to burn when the chamber was opened.

To clean the source: every flange was removed from the source chamber and the flanges were washed by brush with water, then dried by the hot wind from the heater, and finally rinced with acetone or ethanol; the surface of the target was mechanically polished with emery and then rinced with acetone; the discharge filament and quartz glasses for the port were replaced by new ones. Cesium oven was detached from the ion source and the residual Cs was cleaned out of the oven. Then the Cs container was cleaned with aceton, and the entire oven was put in place of the ion source and heated up to 300 °C by the heater wire wound around the oven.

After reassembling, the ion source was pumped down to 10^{-6} Torr. To further clean the ion source, the source was baked by the following procedure. Argon gas was introduced to about 1 mTorr and Ar plasma was produced. Discharge voltage and current were 45 V and about 200 mA, respectively. Target bias was less than 30 V to suppress Au deposition onto the glasses of ports by sputtering. The chamber wall and both flanges were heated by the hot water flowing system and radiation from the discharge filament. The Cs oven was wrapped by wire heaters and asbestos mats at this time to bake out Cs oven entirely. The baking was continued at least for 3~4 hours until the source pressure became below 3×10^{-6} Torr.

(b) Cs loading of the Ion Source

Dry argon gas was used to bring the chamber pressure up to atmosphere. After the valve was closed, the Cs oven was detached from the source and put into a glove box which was filled with He gas. One gram of Cs (99.9 % pure) was put into the Cs container cup of the oven, and the container cup was attached to the oven. The Cs oven was put on its position on the ion source, which had been continuously purged with dry nitrogen. Immediately after the oven was attached, the system was pumped down and the oven valve was opened.

About 2 hours of pumping brought the ion source pressure down to about 10^{-6} Torr. Baking was not done after this pumping to keep the quartz glass of the port clean for higher transmissivity of the laser beams.

(c) Set up of the work function measurement system

Collimation and power measurement of the laser lights were usually done when the ion source was reassembled after its cleaning procedure. The Ar^{+} and He-Ne laser were turned on at least more than 30 minutes before the collimation to avoid the slow drift of the light axes which was associated with the heat of the light sources. Two light choppers were put into the light path and parts of the laser powers were reflected to the detection spot of two photo-diodes. Also parts of the laser powers were monitored by laser power meter with frequency calibrated. Then, the fast light chopper turned on at the

corresponding frequency and the collimation and power measurement of two laser lights were started. Here, the respective ratio of the power measured on the target to the power monitored by the glass was obtained for later data analysis.

The constants of phase sensitive detection circuits were properly adjusted. The input voltage of the reference signals detected by the photo-diodes must be amplified above the lower detection limit of each Lock-in Amplifier.

(d) Start-up of the ion source

The discharge voltage was set to 45 V to avoid producing multiply charged Ar ions. The discharge current was under 100 mA to observe sputtering phenomenon during the sputtering. The target current was 1~2 mA for the upper limit of the target voltage which was restricted to measure the correlation of the work function and Au^- current production rate and to keep the work function constant.

When the argon gas pressure was 1 mTorr, the argon plasma was produced. The parameters of the plasma produced in this discharge condition was not measured. From the measurement performed in larger ion source, the parameters, electron density and electron temperature, were expected to be 3×10^9 /cm^3 and 2 eV, respectively.

§4. Results and Discussion

(4-1) Two-wavelength measurement of Au^- production

(a) Reflectivity measurement

To observe the influence of the condition of the gold surface on the absorptivity of laser lights, the ratio of an injected laser power to a reflected light power on the gold target was measured. An injected laser light passed through an injection port and was reflected on a gold target surface.

A reflected light was monitored by a 2.5 cm diameter power meter after it passed through an exit port. The laser light was injected at 45° with respect to the target surface. The incident photon energies were 1.96 eV for He-Ne laser, 2.40, 2.47, 2.52, 2.54, and 2.61 eV for Ar^+ laser, respectively. Two surface conditions, (1) smooth as-received sample, and (2) rough after a mechanical treatment with emery, were tested.

The measured dependence of the reflectivity upon the incident photon energy is shown in Fig. 11. The reflectivity decreased for a higher incident photon energy. For an as-received gold surface, the value was higher than that of a polished one. This difference was caused mainly by the diffuse reflection on a polished gold surface. The

following experiments were performed with the polished gold surface.

The reflectivity of a cesium-covered gold surface was also measured during the source operation. It was typically 24 % for He-Ne laser and 8 % for Ar^+ laser.

(b) Correlation of work function and Au^- production

Figure 12 shows an example of the time evolution of the photoelectric current induced by the Ar^+ laser and the He-Ne laser, the corresponding monitored laser powers, the target current, and the Au^- current during the source operation. To see the process wherein the work function of the target surface was changed by the decrease of cesium coverage caused by Ar^+ sputtering, the time variation of these variables was monitored simultaneously.

The difficulties in performing this measurement were to decrease the work function lower than 1.96 eV and to observe the slower change of the work function change in this region. This difficulty mainly depends on the control of the cesium deposition on the target. The higher introduction of the cesium vapor into the chamber made a higher deposition on target and prevent the Au^- formation by the sputtering. The less cesium deposition was considered to be sputtered out in a short period or was not observed by observing the p. e. The potential of the plasma detected by a Langmuir probe was a measure of the cesium introduction to the chamber. Whenever the oven was opened to introduce the cesium, the potential of the plasma detected by

the probe was decreased.

To overcome these difficulties, cesium deposition was controlled by the cesium recycling from the wall. First of all, the cesium was deposited heavily on the wall of the chamber. This cesium was considered to be removed both by the interaction to the plasma and by the heat of the wall. The removed cesium drifted through the plasma and deposited on the water cooled target surface. The detailed handling of the oven for cesium introduction was described in chapter 3-1.

The number and the energy of Ar^+ which sputter the cesiated target was controlled by the discharge current and the target voltage, respectively. The discharge power was kept lower to keep the constant work function and a slower change of the p. e.

All experiments described here were performed after keeping the work function constant and then changed only one sputtering parameter, the discharge current or the target voltage. Firstly, the experiment was performed by controlling the discharge current because it was the most controllable and effective parameter for the discharge.

When the condition that $I_d > 100$ mA, p. e. decreased in a short period because the cesium was sputtered by the higher number of the sputtering atoms. Then to deposit the cesium, I_d was kept about 10 mA until p. e. by Ar^+ laser was detected. After the p. e. by Ar^+ laser became constant, I_d was increased and the same measurement was

started. By measuring the change of both p. e, monitored laser powers, I_t and Au^- current in time, the correlation between Au^- production rate and the work function was obtained.

The Ar plasma was operated under the conditions of an arc power of I_d = 61 mA, V_d = 45 V, a target voltage V_t = - 200 V and a gas pressure of 1 mTorr. Cesium introduction was terminated but a small amount of cesium was still deposited on the target surface due to the recycling from the wall of the ion source.

A target current and monitored laser powers were nearly constant but two photoelectric currents decreased with time. From the ratio of the two photoelectric yields, the time-dependence of the work function was obtained by using eq. (4). Here, the change in the reflectivity of each laser light due to the cesium deposition was considered.

From the integration of the measured vertical profile of the beam, the total Au^- current was estimated to be 400 times larger than the detected Au^- current, assuming the beam was cylindrically symmetric. The correlation between a negative ion production rate and a work function is shown in Fig. 13. Here the negative ion production rate was defined to be Au^- current / target current. The highest Φ_w obtained in this experiment was 1.89 eV. The Φ_w of a gold surface in an Ar plasma with weak cesium introduction was reported to decrease to 1.5 eV, utilizing two different wavelength lasers alternately without correcting the absorptivity.[4] In the present experiment, the lowest work function was 1.34 $\pm$ 0.07 eV. The negative ion production rate slightly decreased for increasing target work function from 1.34 to 1.89

eV. The negative ion production rate was 3.2 % (Au^- current = 40.7 μA, target current, I_t = 1.28 mA) when the target work function was 1.34 eV.

If we assume the initial barrier of the potential and the potential width as those fitted to H^-, D^-, and Mo^- data, then the Au^- production rate would change by a factor of 3 ~ 11 for the change of 0.5 eV in this work function region. However, our observation indicated change of only a factor of 1.2. This deviation was considered due to saturation of negative ion production rate at a low Φ_w region, as Yu showed in the case of $^{16}O^-$.[15)]

The error was within ± 4 % for the Au^- production rate and that in determining work function was within ± 5 % considering the scatter of the data signals caused by the plasma noise.

The ambiguity in determining the lowest work function by correcting the reflectivity are follows. As the work function becomes small, the ambiguity between with and without considering the reflectivity becomes large. The lowest work function determined with the method by correcting the reflectivity (method A) was in - 8 % of the one gained by the method which does not consider the reflectivity (method B). The work function obtained by correcting the diffuse reflection (method C) becomes less than + 18 % of that determined by the method B. However, the work function determined by correcting the following factors becomes within - 3 % of the one obtained by the method A. The two factors must be considered, (1) by the cesium

deposition on the target surface, the reflectivity becomes 40 % of that gained by the polished surface and (2) by the diffuse reflection effect, the real reflectivity is a double of the value showed in Sec. 4-1. (a).

When the work function was 1.9 eV, the ambiguity was less than 0.6 % for any method.

4-2. Au^- measurement under the constant work function

(a) Effect of the discharge current on Au^- production

Figure 14 shows the effect of discharge current which changes the number of incident Ar^+ on the Au^- production rate when the work function was constant. The discharge conditions were Ar 1 mTorr, V_d = 45 V, and V_t = - 200 V, and Φ_w was kept at 1.3 eV, which was the lowest Φ_w value observed. Under the constant Φ_w condition, both the target current and the Au^- current was proportional to the discharge current, while the negative ion production rate did not depend on the discharge current. The negative ion production rate was estimated to be 3.4 %. The error was within ± 4 % for the Au^- production rate and within ± 1 % for discharge current. The main error was the scatter of the data signals caused by the plasma noise.

(b) Au^- production dependence on the target voltage

The effect of the target voltage which changed incident energy of Ar^+ on the Au^- production was studied under the constant work function condition, as shown in Fig. 15. The solid line is the calculated sputtering yield.[19] The experimental conditions were the following: Ar 1 mTorr and V_d = 45 V, and Φ_w was kept at 1.8 eV. The negative ion production rate increased as the target voltage increased. This

tendency is qualitatively similar to the calculated sputtering yield curve.

4-3. Energy distribution of Au^- beam

The energy spectrum of the Au^- beam was measured to see the applicability of Au^- beam to a H. I. B. P. method when the ion source was operated with an argon plasma under the following conditions; the discharge voltage (V_d) was 45 V, the discharge current (I_d) was 16 mA, and the argon pressure was 1 mTorr. An example of the experimental result is shown in Fig. 16. The solid line is a detected negative ion current; I^-. Closed circles show the derivative of I^- with respect to the retarding potential, dI^-/dE. We determine the energy spread, ΔE, as the F. W. H. M of the curve of dI^-/dE.

Energy spectra of Au^- produced by the Ar^+ ions of bombarding energies from 100 to 279 eV are presented in Fig. 17, where the distributions have been normalized at the peak. The higher bombarding energy was possible (< 500 eV), but in this experiment the local discharge between the cesiated target surface and the filament happened. This limited the higher bombarding energy of this experiment. As shown in Fig. 17, it is evident that the higher energy components of the kinetic energy distribution became small as the target voltage was decreased.

Brizzolara *et al.* had measured the kinetic energy distribution of the neutral Cu atoms sputtered by normal incident Ar^+ ions from the

Cu surface, and reported that higher energy components of the kinetic energy distribution decreased as the incident energy of Ar^+ ions were decreased when the incident energy was less than 600 eV[20]. This suggests that the energy spectrum of gold atom sputtered by Ar^+ ions shows the same tendency.

The energy spreads observed are plotted as a function of the target voltage (V_t) in Fig. 18. The ΔE increases with increasing V_t. The uncertainties in determining the ion energy are as follows. The maximum energy component in the perpendicular direction to the beam is 0.19 % of the total beam energy considering the incident angle of the beam defined by the collimating aperture. And the deflection due to stray magnetic field causes maximum error of less than 0.02 % of the beam energy. The error resulting from the F. W. H. M of the curve of dI^-/dE is below 0.24 V because the energy spread corresponding to each channel is 0.12 V. Therefore the error in determining the energy spread ΔE was estimated to be less than 9 %. The measured energy spread was less than 10 eV for V_t lower than 300 V. The maximum Au^- current density (Au^- current / target surface area) was 9.2 $\mu A / cm^2$ when the cesiated target work function was 1.34 eV, I_d = 61 mA, V_d = 45 V and V_t = -200 V.[21] With these values, the application of a Au^- beam from the plasma-sputter type negative ion source to the potential fluctuation measurement seems feasible.

§5. Summary

An *in situ* method which was able to determine the work function as a function of time by measuring photoelectric currents induced by a He-Ne laser (632.8 nm) and an Ar^+ laser (488 nm) simultaneously was developed. Following experiments were performed with this method to measure the work function of a target surface in a negative ion source during source operation. The reflectivity at each wavelength on a cesiated gold surface in an Ar plasma was measured and was taken into account in determining the work function of a cesiated gold surface.

The dependence of Au^- production upon the target work function of a plasma-sputter-type negative ion source was studied. The work function of a clean gold surface is known to be 5.3 ~ 5.5 eV.[11] By introducing cesium on the gold surface, it was decreased down to 1.3 eV. The negative ion production rate (Au^- current / target current) slightly decreased for target work function increased from 1.3 to 1.9 eV (Fig. 13). In this work function region, the negative ion production rate seemed saturated. This was considered to be as Yu showed in the case of a low Φ_w region of $^{16}O^-$, that the production rate of Au^- was saturated. The maximum Au^- production rate (Au^- current / target surface current) was 3.2 % when the cesiated target work function, discharge current I_d discharge voltage V_d and target voltage V_t were

1.34 eV, 61 mA, 45 V and -200 V, respectively.

Under the constant work function of a cesiated gold surface in an Ar plasma, both the Au^- current and the target current increased in proportion to the discharge current, in the range of the discharge current of less than 0.1 A. This corresponds to the constant negative ion production efficiency (3.4 %) as shown in Fig. 14.

The negative ion production rate increased as the target voltage increased from 100 to 200 V when the work function was the same (1.8 eV). This tendency was qualitatively similar to the reported sputtering yield curve.

Using a retarding potential type electro-static analyzer, the energy distribution function of Au^- produced in a plasma-sputter type negative ion source was measured to see the applicability of Au^- beam to the H. I. B. P. method. The higher energy components of the distribution decreased therefore the energy spread ΔE which was defined to be a F. W. H. M of the energy distribution function of Au^- decreased as V_t was decreased. The higher energy component in the energy spectrum of the Cu atoms sputtered from the Cu metal by Ar^+ ions decreased as the incident ion energy decreased. This suggests that the energy spectrum of the sputtered gold atom by Ar^+ ions shows the same tendency. For V_t lower than 280 V, ΔE was under 10 eV. The maximum Au^- current density on the target was 9.2 $\mu A / cm^2$. With the values of the energy spread and the beam density, a beam of Au^- seems applicable to a H. I. B. P. method.

References

1) G. D. Alton, Y. Mori, A. Takagi, A. Ueno and S. Fukumoto:
Nucl. Instrum. & Methods. **A270** (1988) 194.

2) Y. Mori, G. D. Alton, A. Takagi, A. Ueno and S. Fukumoto:
Nucl. Instrum. & Methods. **A273** (1988) 5.

3) Y. Mori, A. Takagi, K. Ikegami, A. Ueno and S. Fukumoto:
Nucl. Instrum. & Methods. **B37/38** (1989) 63.

4) M. Sasao, Y. Okabe, J. Fujita, M. Wada and H. Yamaoka:
Rev. Sci. Instrum. **61-1** (1990) 418.

5) C. Hosea, F. C. Jobes, R. L. Hickock and A. N. Dellis:
Phys. Rev. Lett. **30** (1973) 839.

6) K. Takasugi, H. Iguchi, M. Fujiwara and H. Ikegami:
J. Phys. Soc. Jpn. **52** (1983) 2389.

7) K. Ishii, H. Inami, T. Kawabe and S. Miyoshi:
Rev. Sci. Instrum. **55** (1984) 1924.

8) G. A. Hallcock, J. Mathew, W. C. Jennings and R. L. Hickok,
A. J. Wootton and R. C. Isler: Phys. Rev. Lett. **56** (1986) 1248.

9) G. A. Hallcock, A. J. Wootton and R. L. Hickok:
Phys. Rev. Lett. **59** (1987) 1301.

10) H. C. Patter and J. M. Blakely:
J. Vac. Sci. & Technol. **12** (1975) 635.

11) H. Yamaoka, M. Sasao, M. Wada and H. J. Ramos:
Nucl. Instrum. & Methods. **B36** (1989) 277.

12) P. Sigmund: Phys. Rev. **184** (1969) 383.

13) M. Wada: Ph. D. Thesis, LBL-Report 15800, Lawrence Berkeley Laboratory, Univ. California, Berkeley (1983).

14) A. Blandin, A. Nourtier, D. W. Hone:
J. Phys. (Paris) **37** (1976) 369.

15) M. L. Yu: Phys. Rev. Lett. **40** (1978) 574.

16) M. L. Yu: Phys. Rev. Lett. **47** (1981) 1325.

17) R. H. Fowler: Phys. Rev. **38** (1931) 45.

18) K. N. Leung, K. W. Ehlers and M. Bacal:
Rev. Sci. Instrum. **54** (1983) 56.

19) N. Matsunami, Y. Yamamura, K. Itikawa, N. Itoh, Y. Kazumata, S. Miyagawa, K. Morita, R. Shimizu and H. Tawara:
At. Data and Nucl. Data Tables, **31** (1984) 75.

20) R. A. Brizzolara, C. B. Cooper and T. K. Olson:
Nucl. Instrum & Meth. **B35** (1988) 36.

21) Y. Okabe, M. Sasao, H. Yamaoka, M. Wada and J. Fujita:
Jpn. J. Appl. Phys. **30** (1991) 1307.

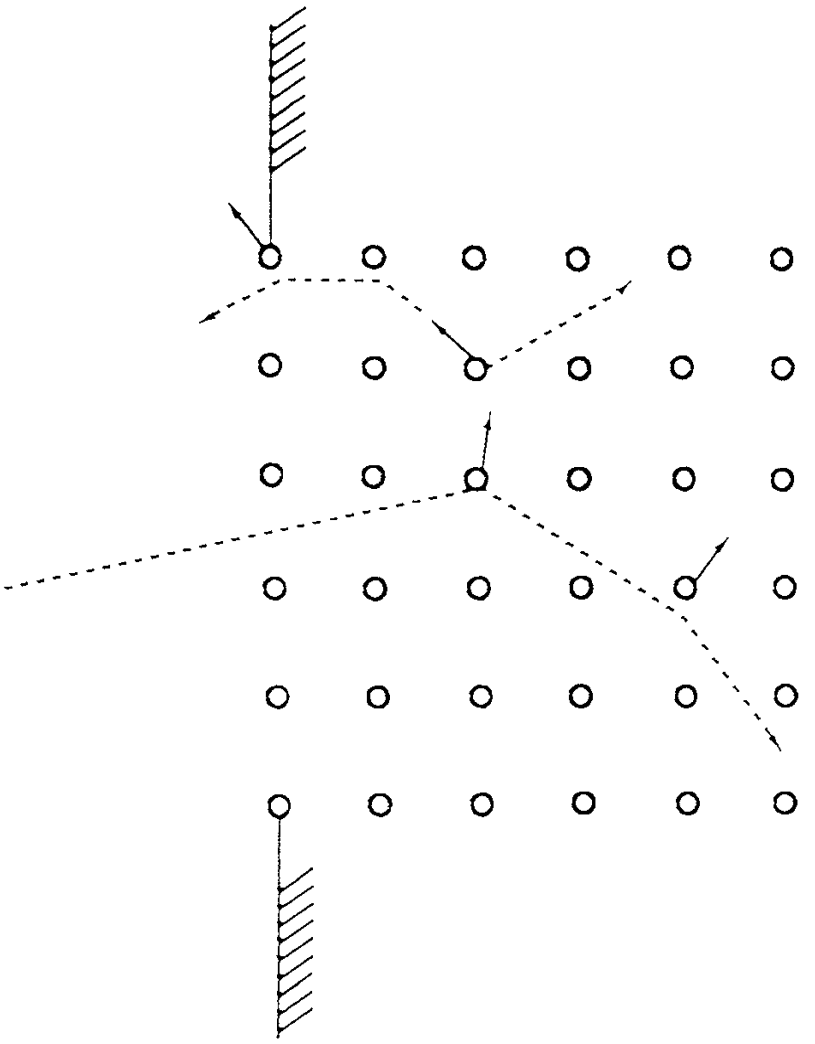

Fig. 1. The example of the linear cascade model. Recoil atoms from ion-target collisions receive sufficiently high energy to generate recoil cascades. The density of recoil atoms is sufficiently low so that knock-on collisions dominate and collisions between moving atoms are infrequent.

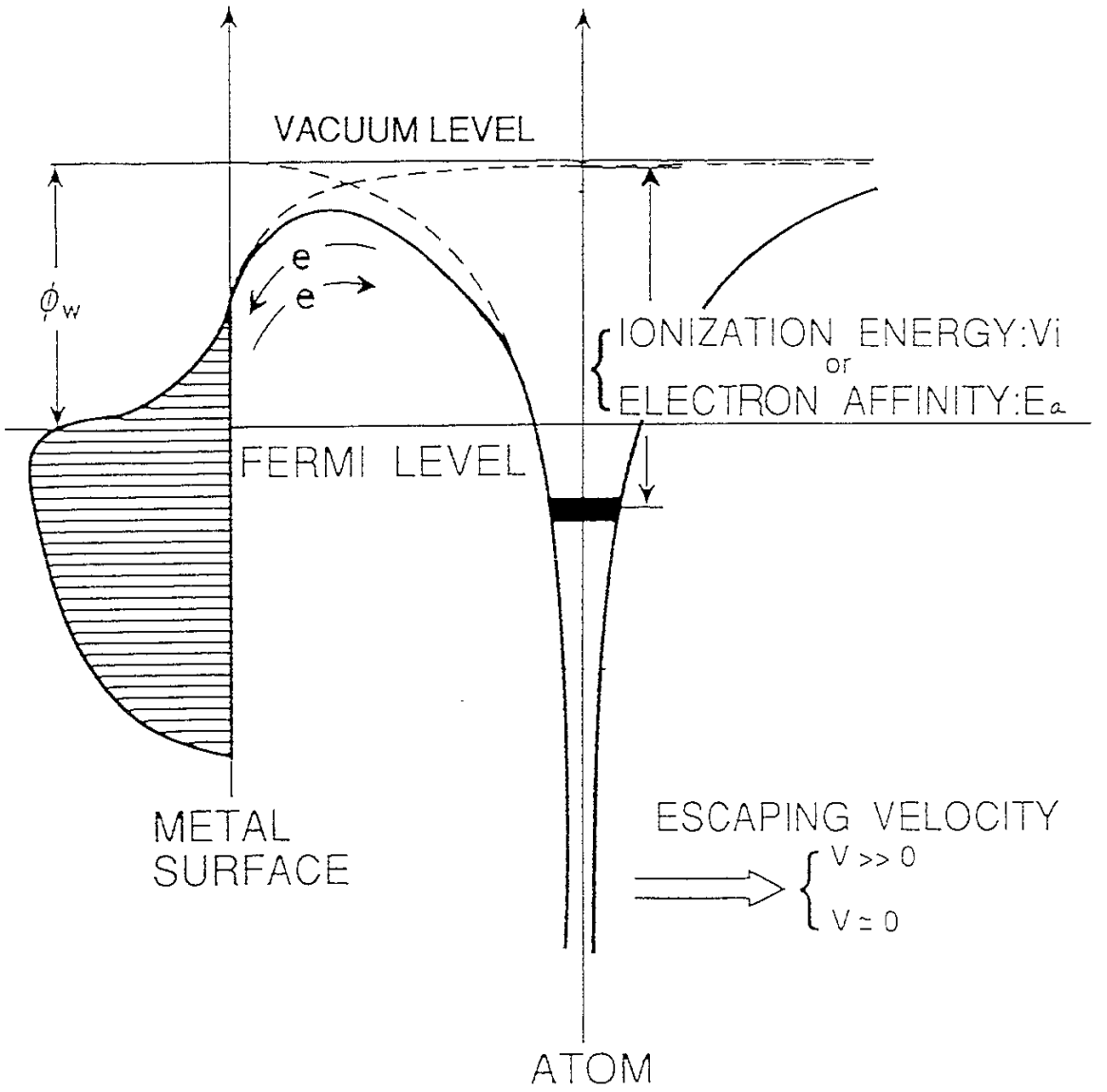

Fig. 2. Potential diagram of a metal and an atom near the metal surface. Φ_w is the work function of the metal and e is the electron.

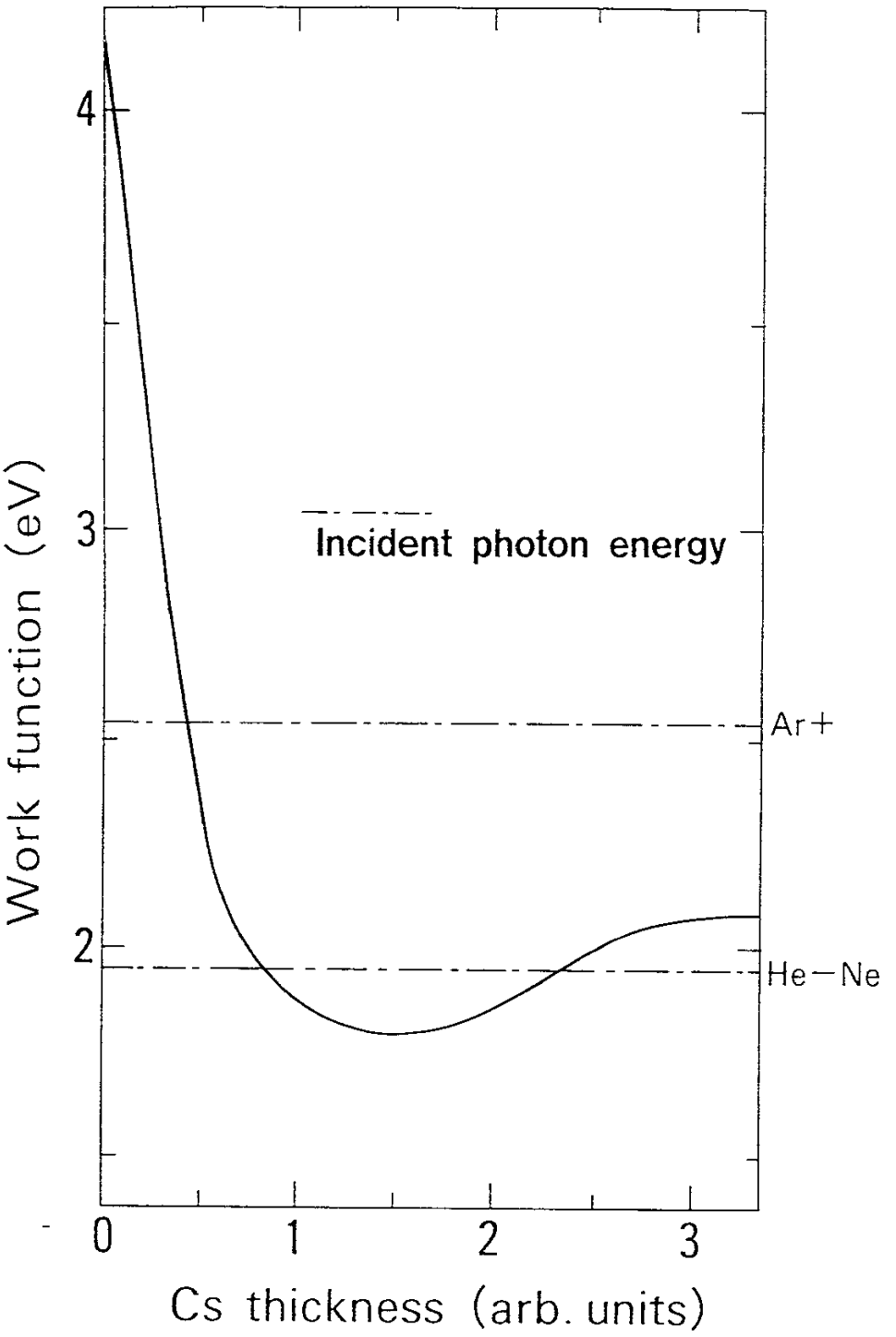

Fig. 3. Change in the work function of Mo covered with Cs (ref. 13).

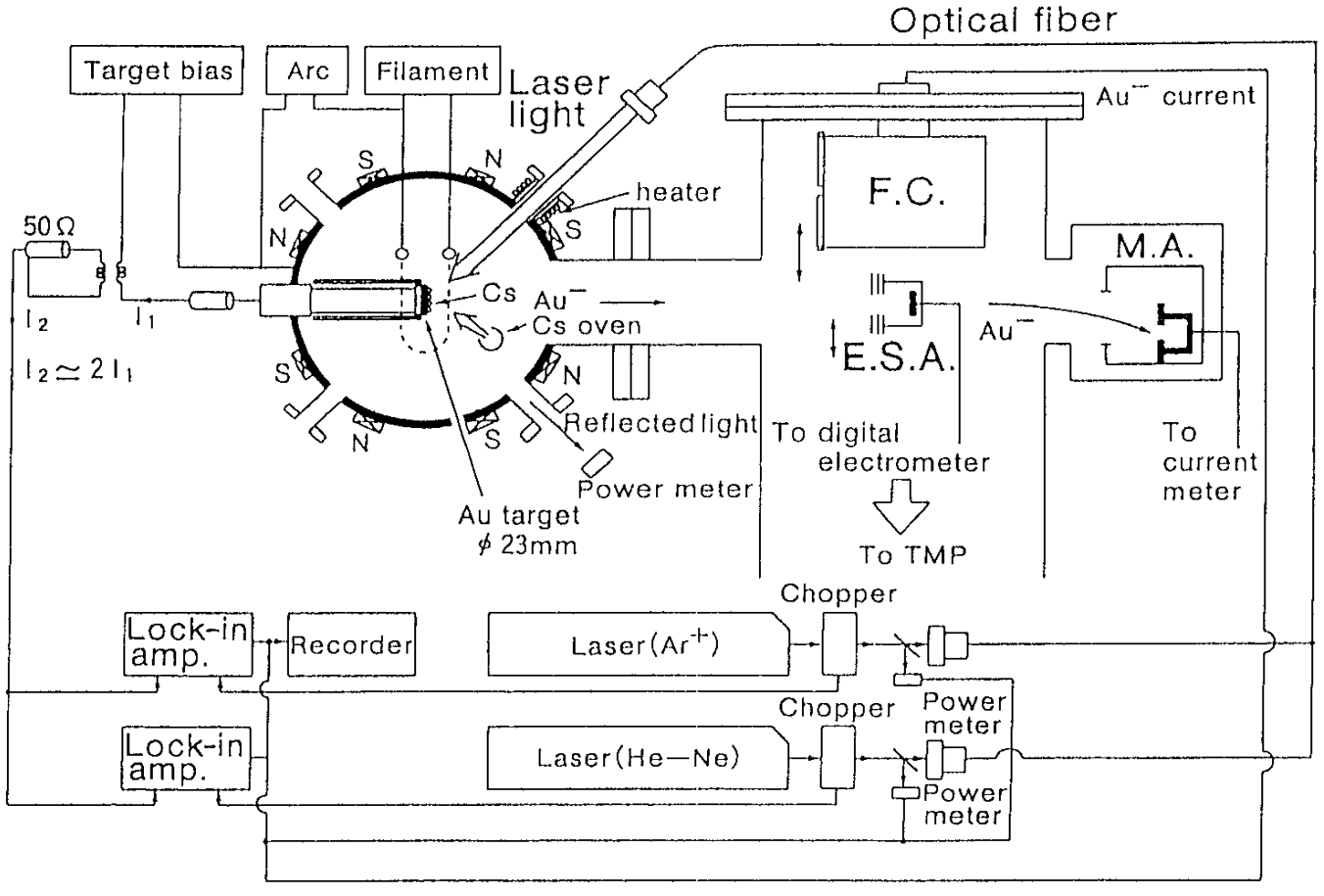

Fig. 4. Schematic diagram of the experimental setup. F. C, E. S. A. and M. A. correspond to Faraday Cup, Electro-Static Energy analyzer and Mass Analyzer, respectively.

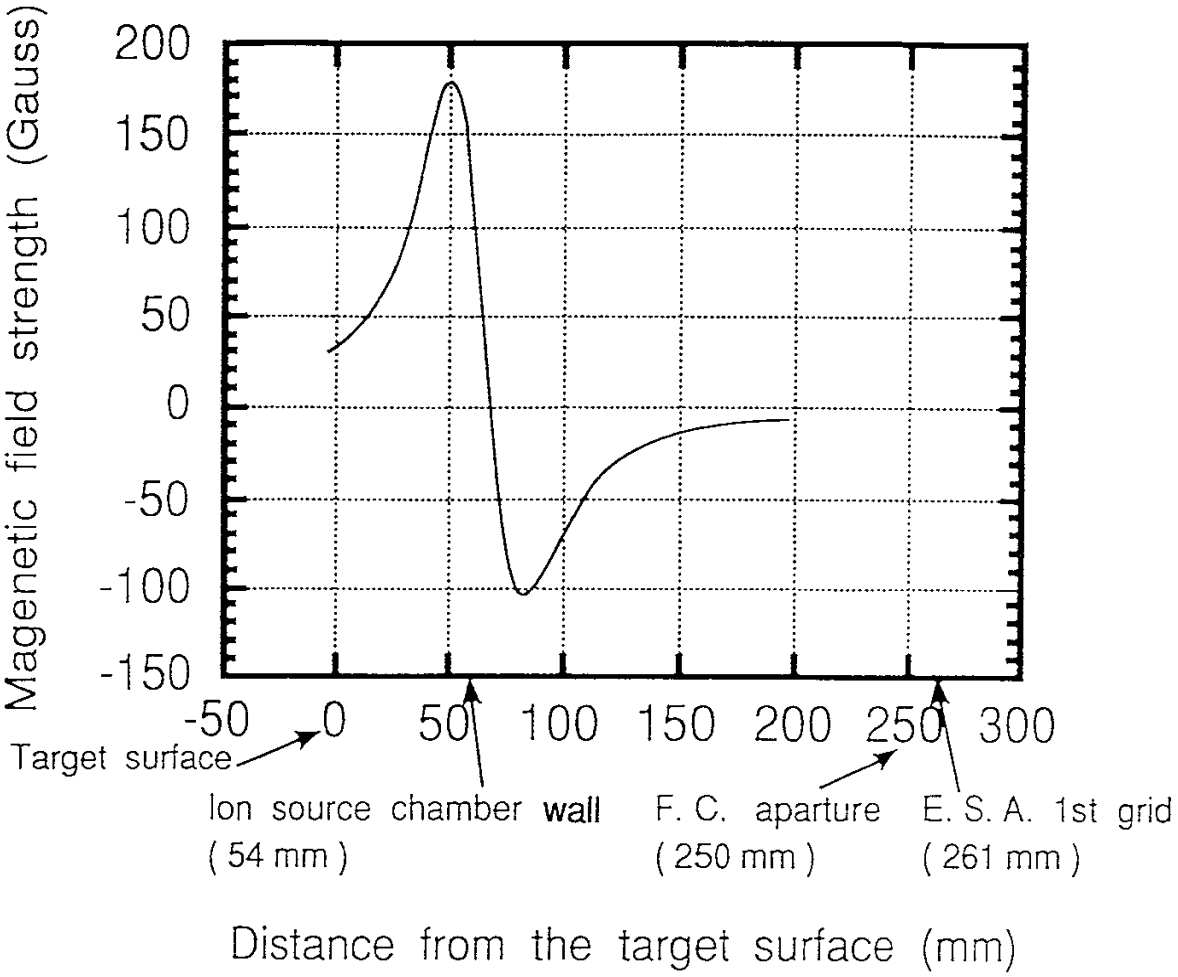

Fig. 5. Spatial profile of the magnetic field in the vacuum chamber.

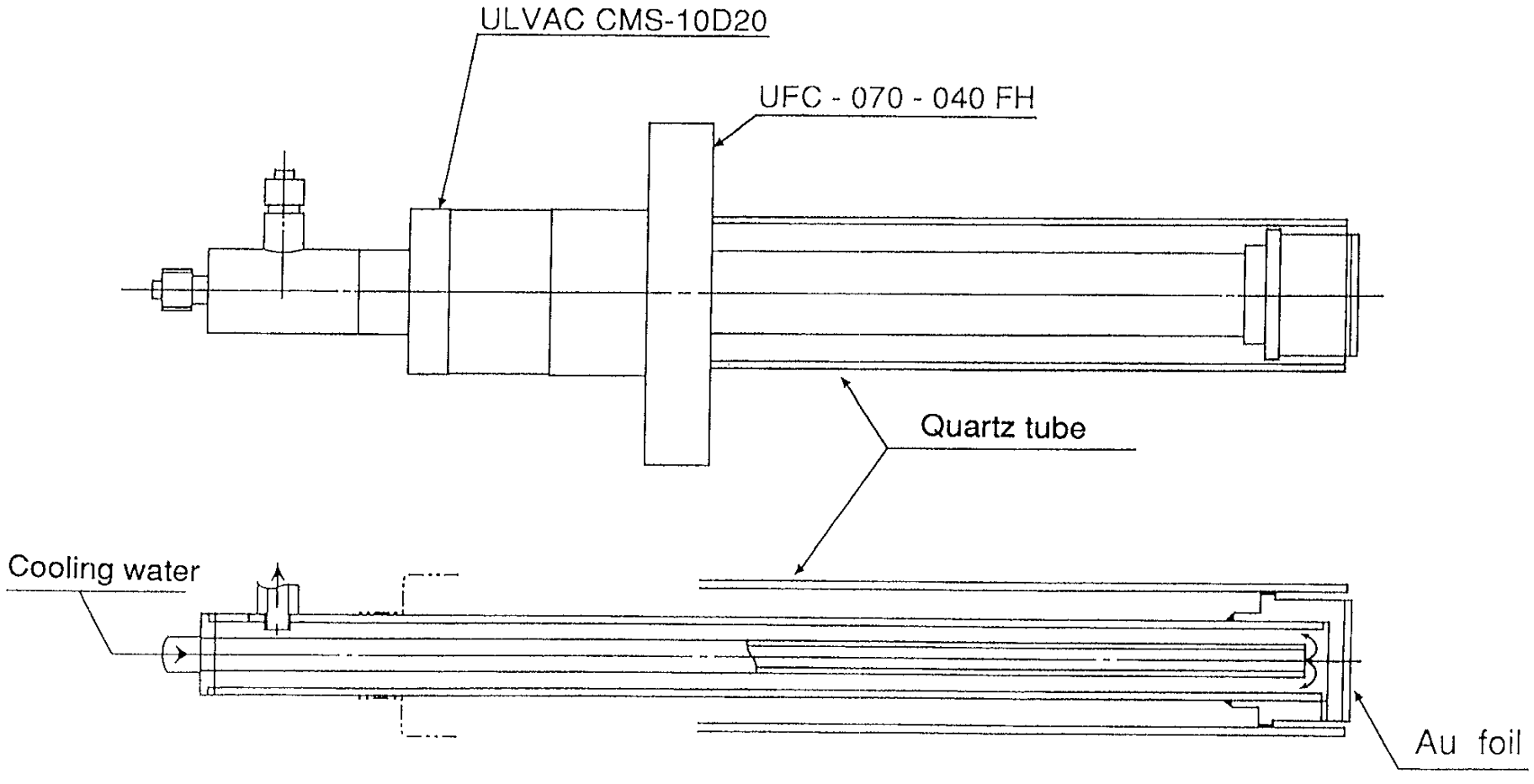

Fig. 6. Schematic diagram and cross sectional view of the target.

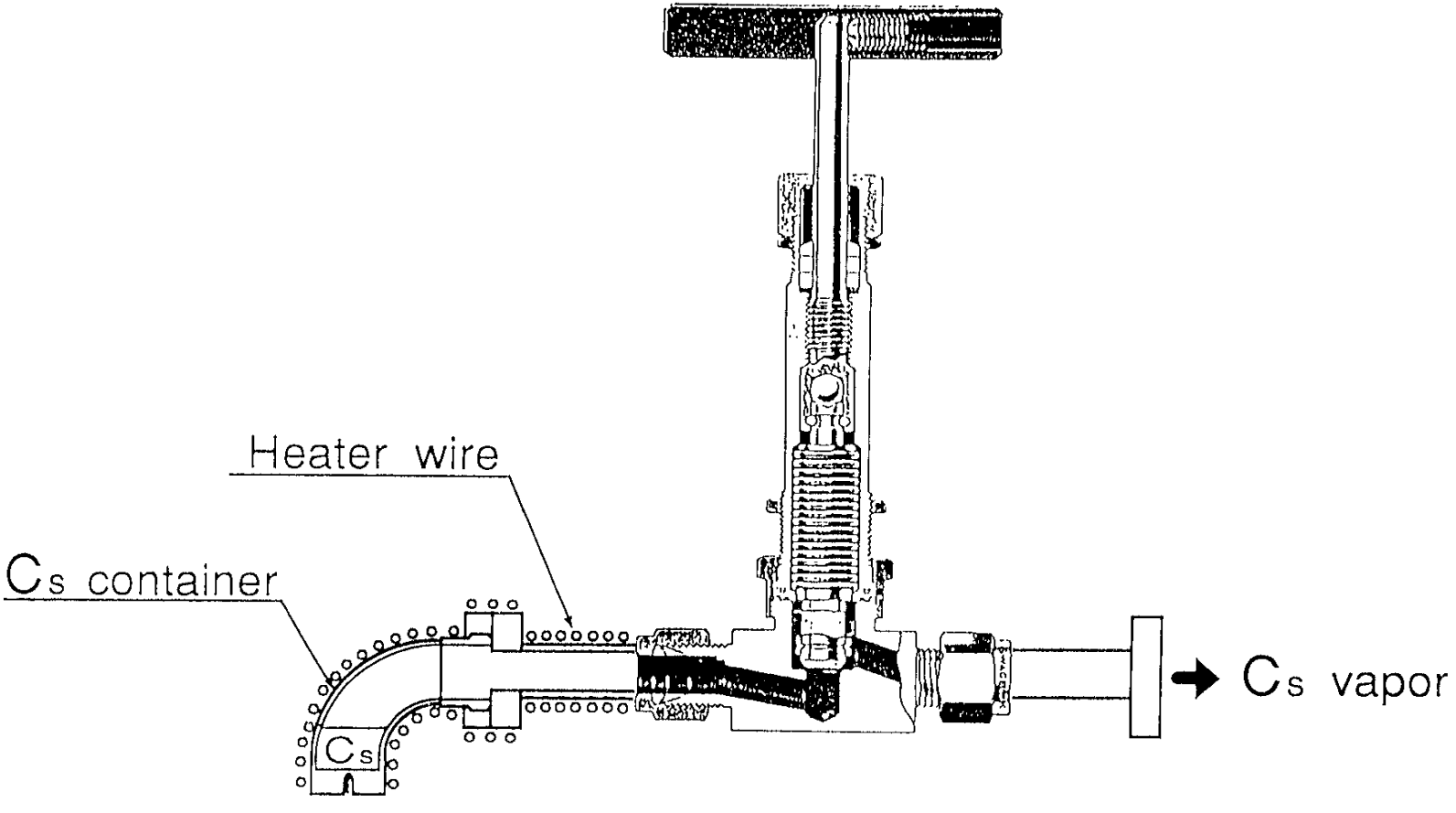

Fig. 7. Cross sectional view of the cesium oven.

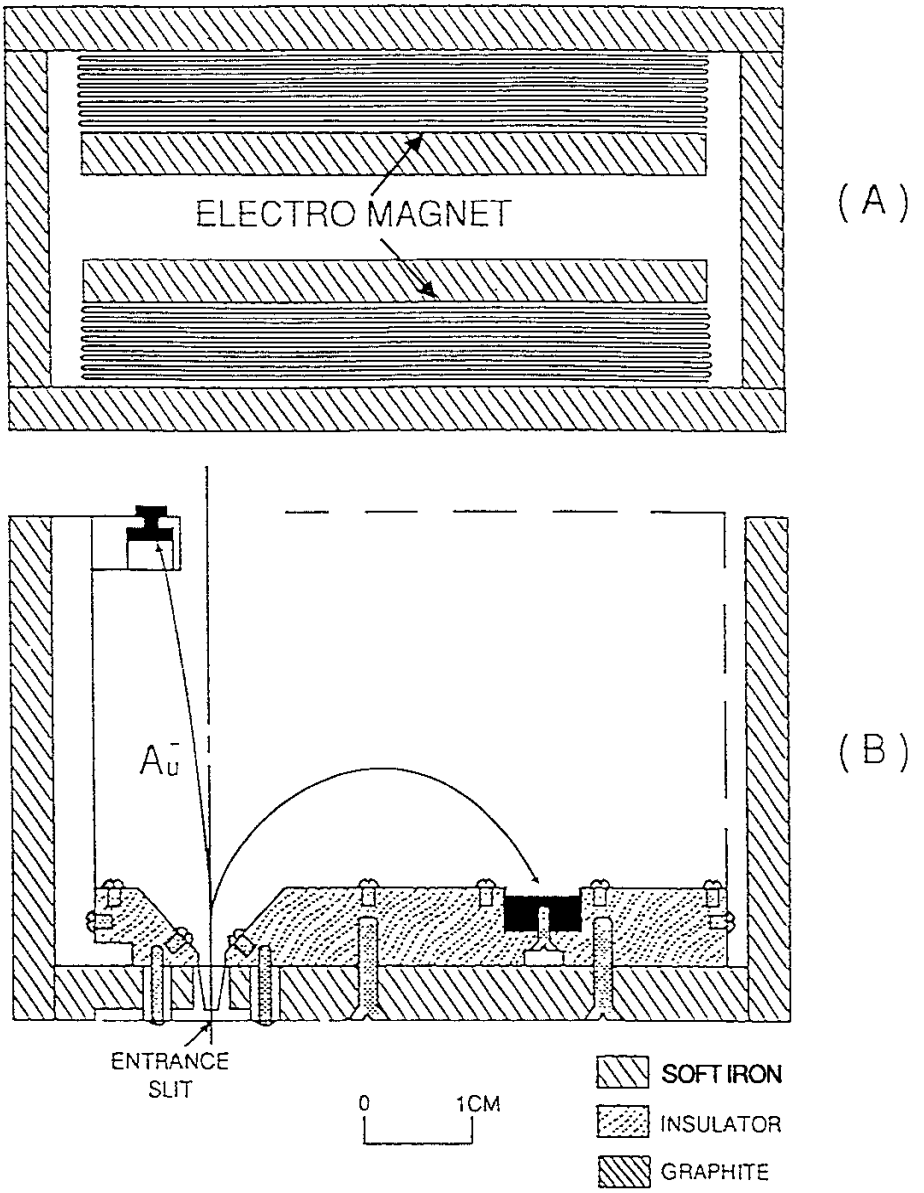

Fig. 8. Cross sectional view of the mass spectrometer.

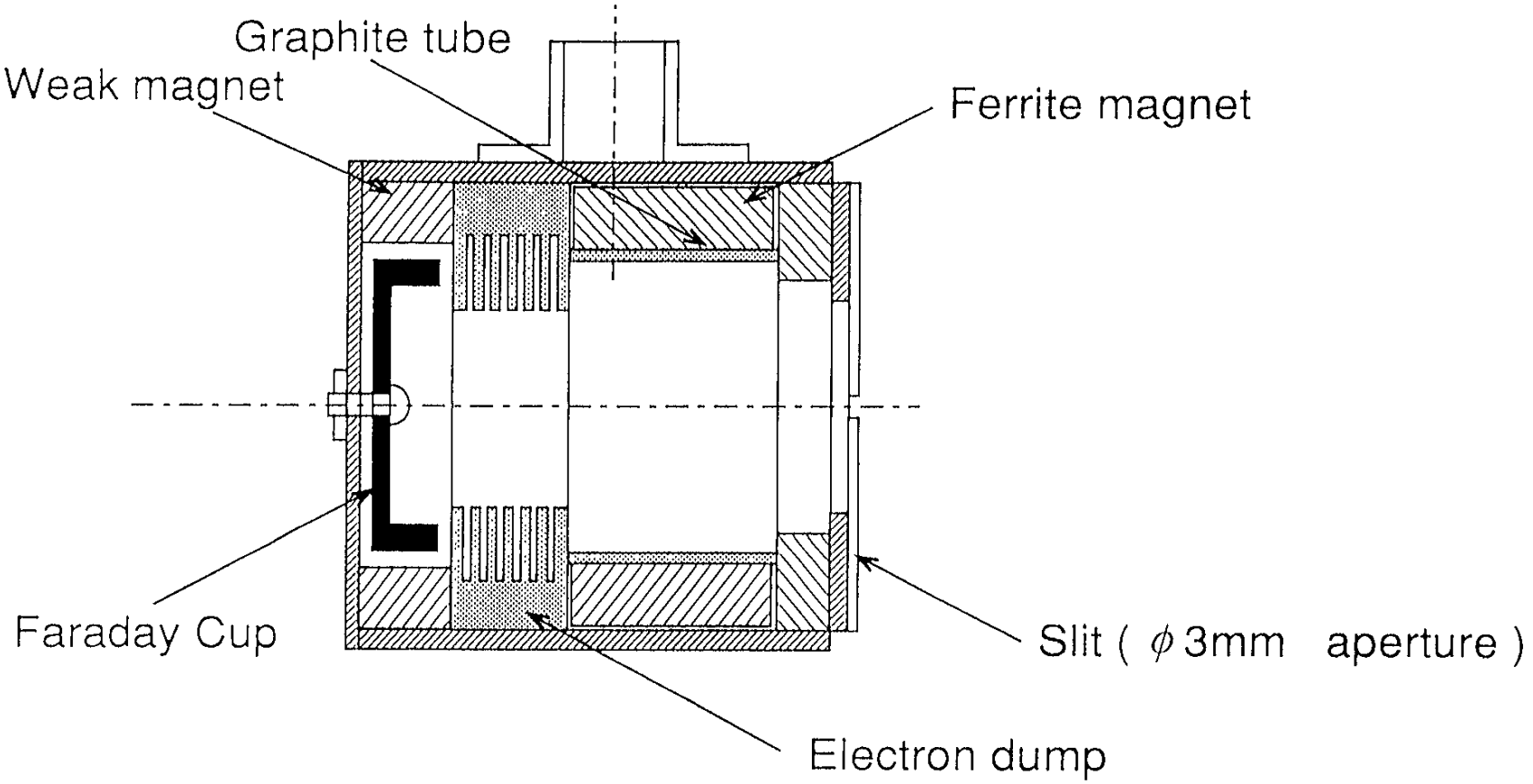

Fig. 9. Cross sectional view of the Faraday cup system.

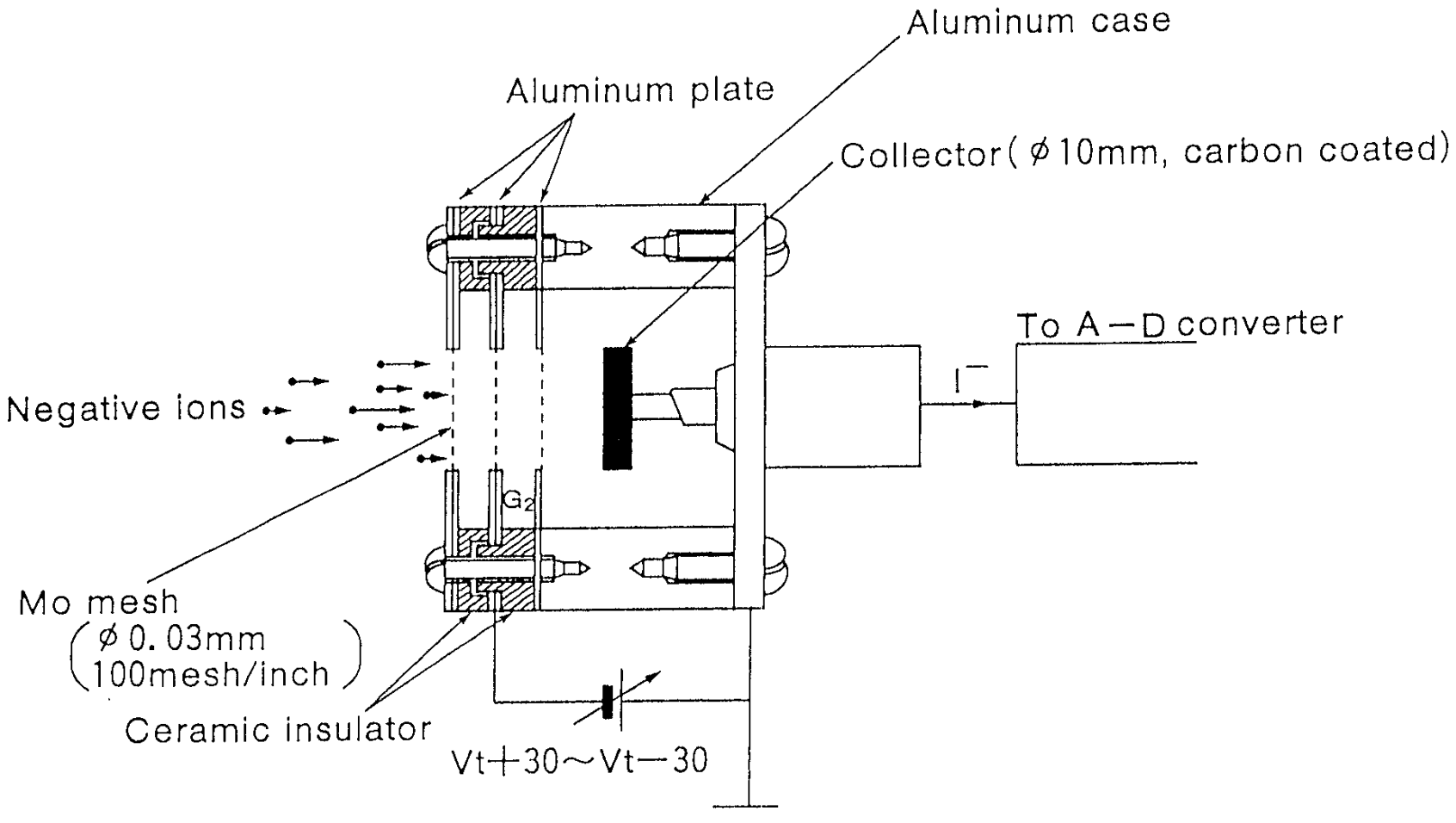

Fig. 10. A schematic diagram of the retarding potential type electric static analyzer.

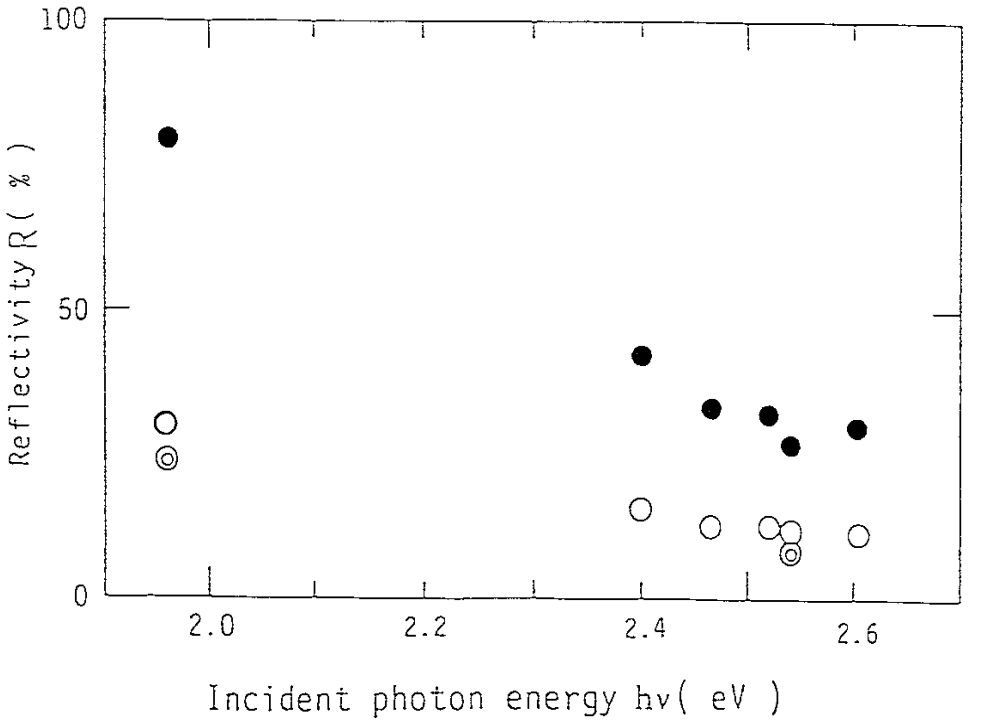

Fig. 11. Change in the reflectivity of gold surface for the different wavelengths of laser light and the different roughness of the surface. ●: as-received, ○: after mechanical treatment with emery, ◎: in Ar plasma with cesium under the experimental condition of Ar 1mTorr, V_d = 45 V, I_d = 61 mA, V_t = - 200 V.

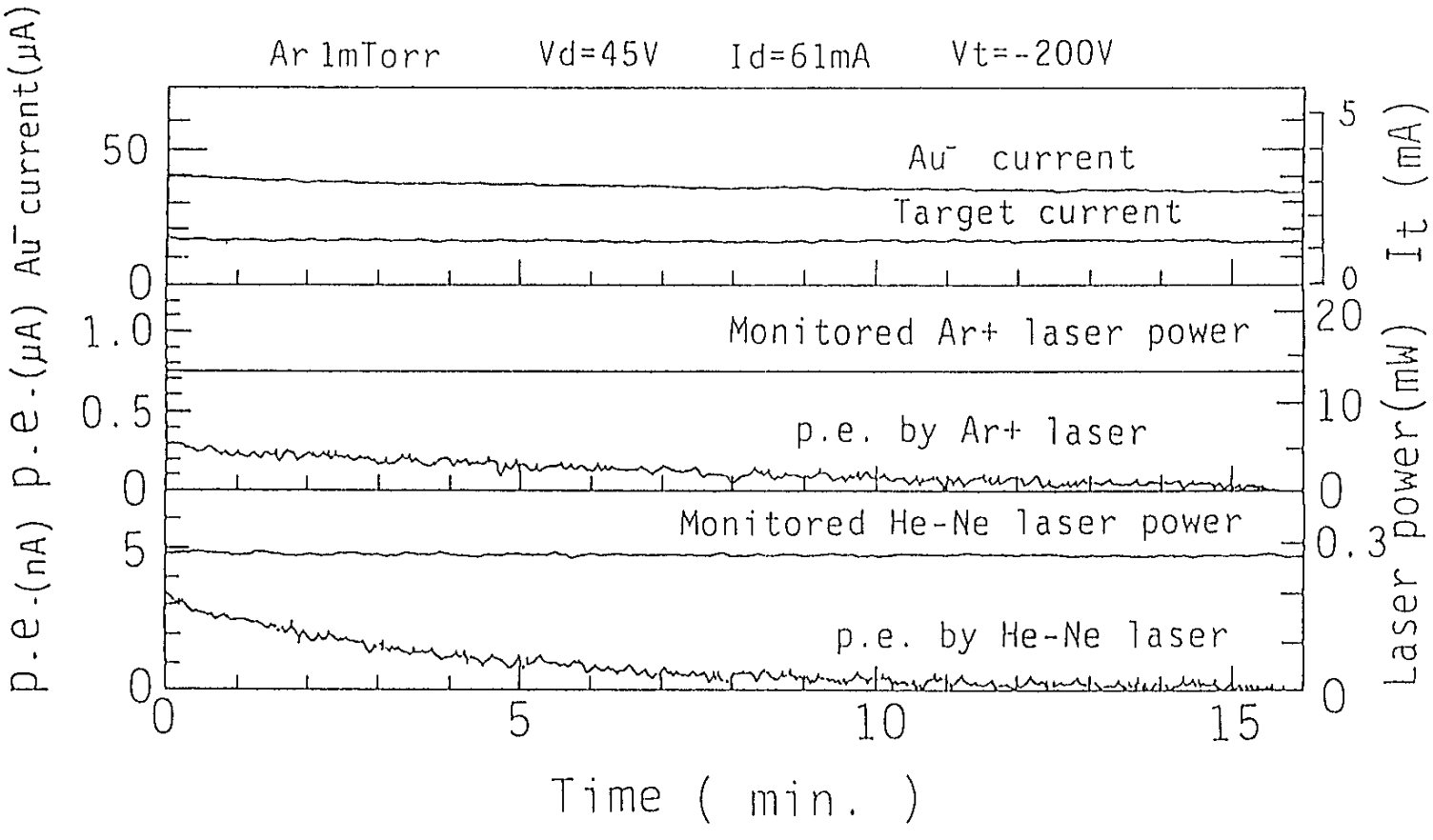

Fig. 12. Time-dependent signal of photoelectric currents p. e, (He-Ne, Ar^+), Au^- current, monitored laser power and target current. The experimental conditions were the following: Ar 1 mTorr, V_d = 45 V, I_d = 61 mA, V_t = - 200 V.

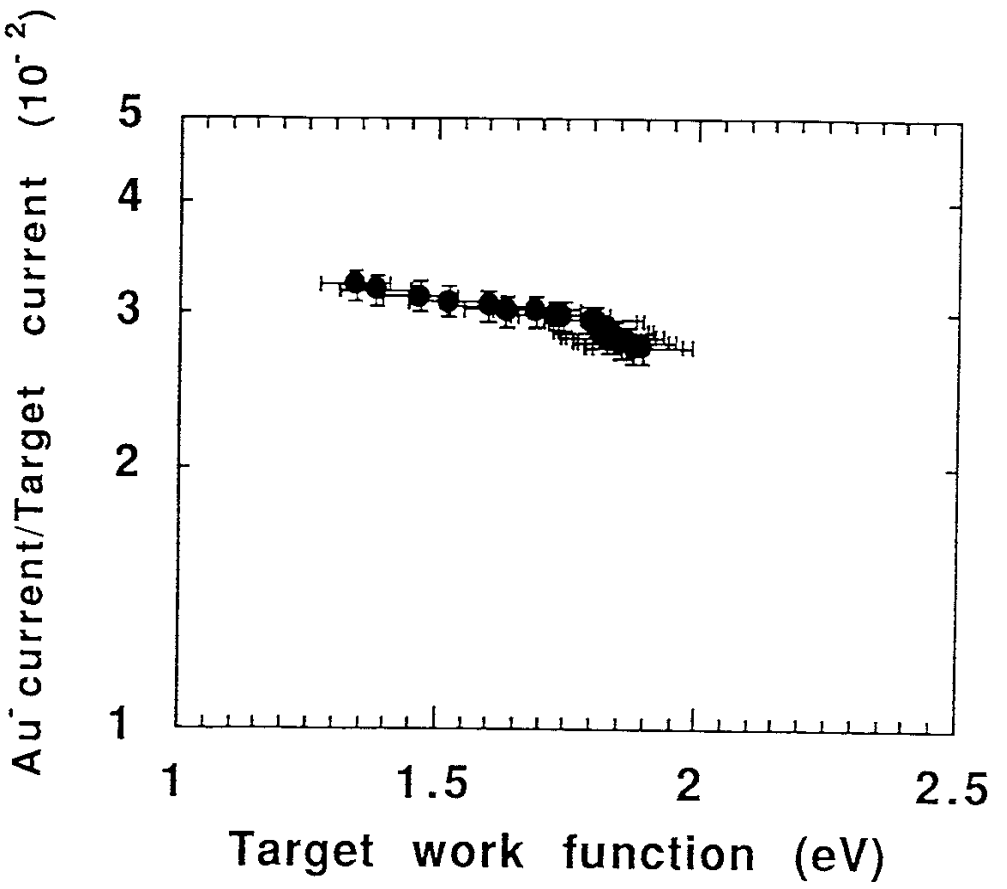

Fig. 13. Correlation between the measured work function and the Au^- production rate. The production rate is defined as the ratio of the extracted Au^- current to the target current. The experimental conditions were the same as shown in Fig. 12.

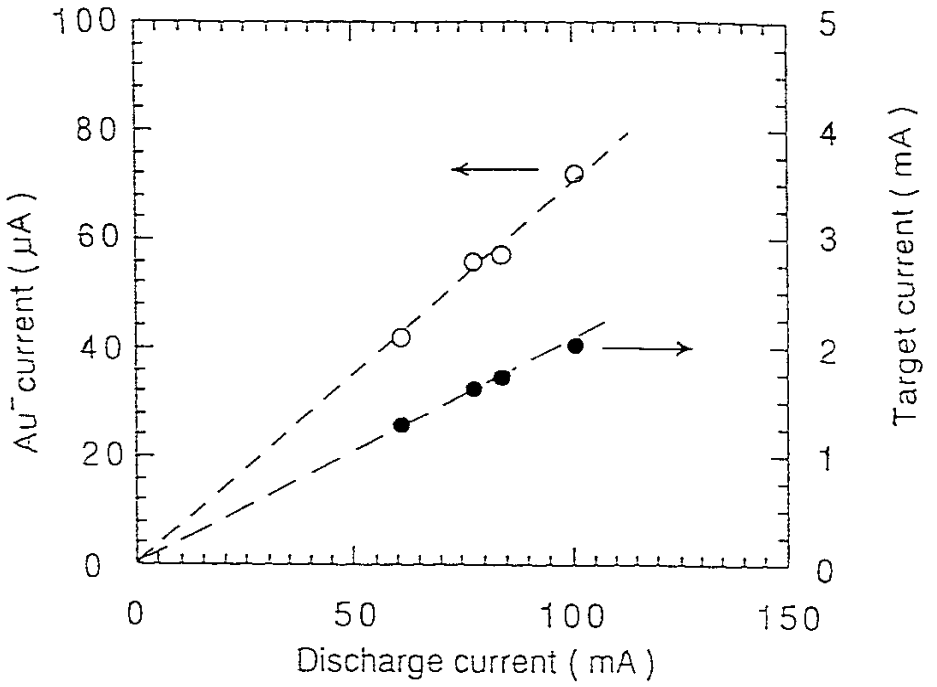

Fig. 14. Effect of the discharge current on the Au- production rate under the constant work function 1.3 eV and Ar 1 mTorr discharge, V_d = 45 V, V_t = - 200 V. ○: Au^- current,●: Target current.

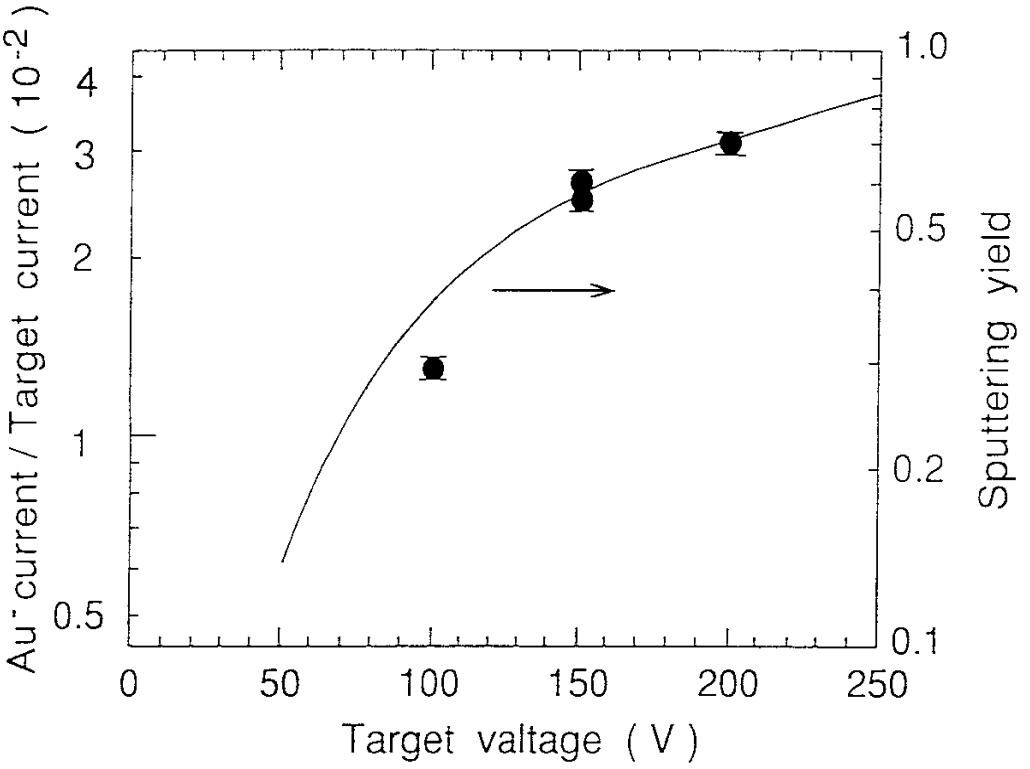

Fig. 15. Effect of target voltage on the Au^- production rate under the constant work function 1.8 eV and Ar 1 mTorr discharge, $V_d = 45$ V. The solid curve represents the sputtering yield.

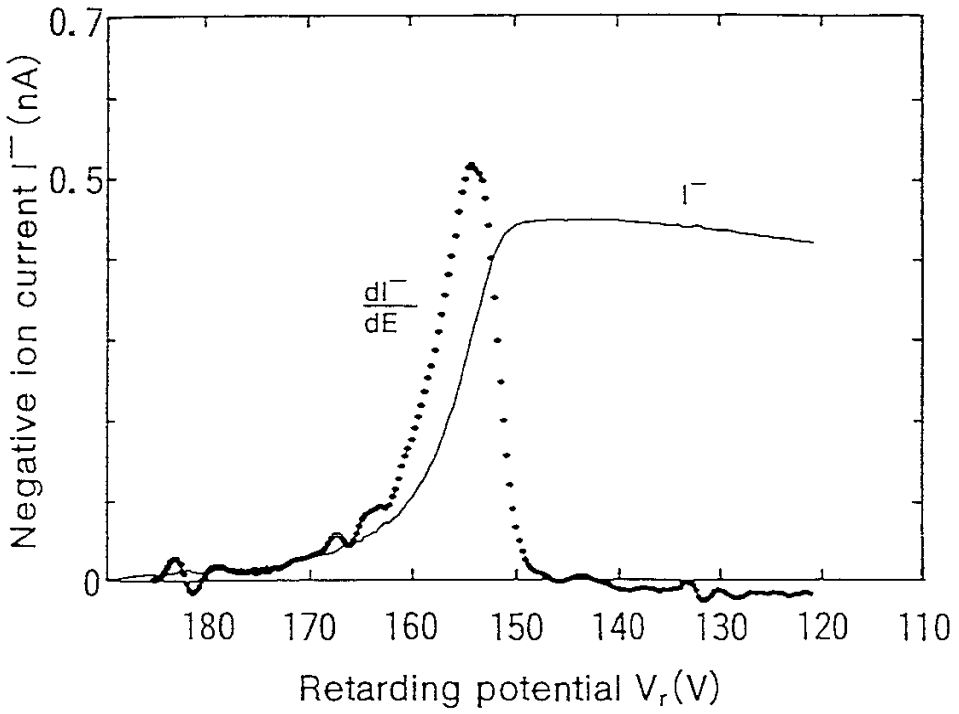

Fig. 16. An example of the *I-V* characteristics of the electrostatic analyzer and the first order derivative of the detected current with respect to the bias voltage to the analyzer. The experimental condition was following; discharge current I_d = 16 mA, discharge voltage V_d = 45 V, Ar 1mTorr.

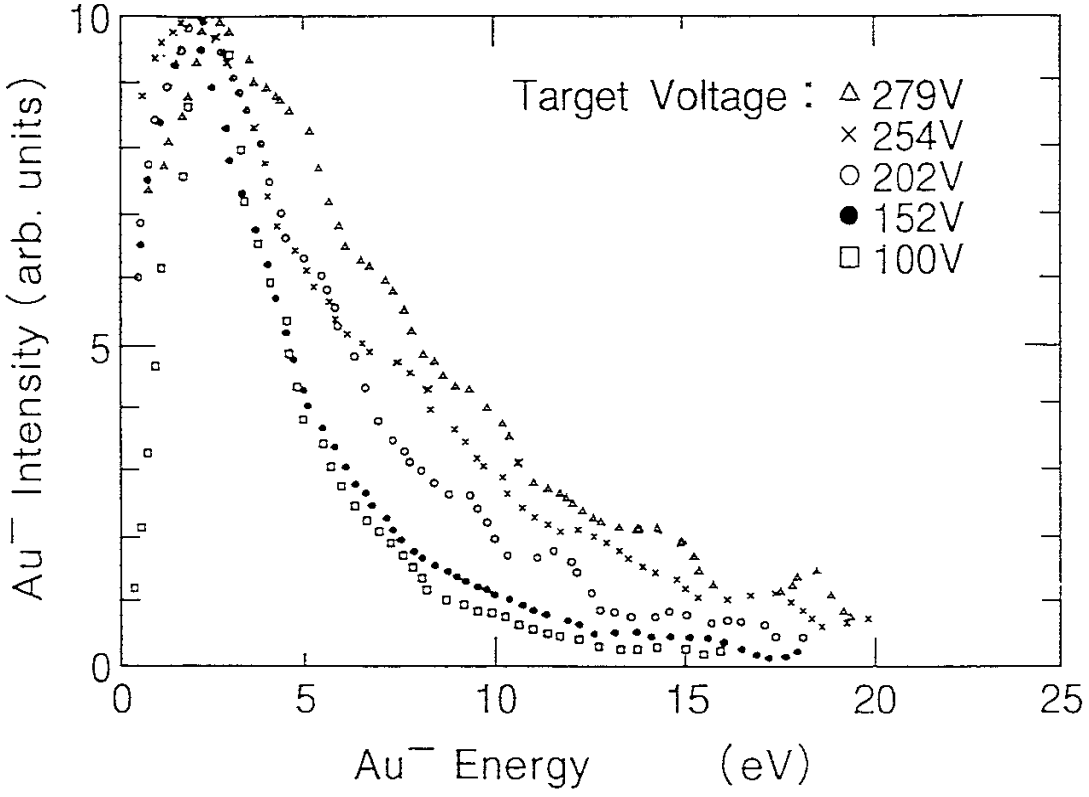

Fig. 17. Kinetic energy distribution of differentiated Au^- current for bombarding Ar^+ ion energies of 279, 254, 202, 152, 100 eV. The curves are normalized to have equal peak heights. The experimental condition was the following; discharge current I_d = 16 mA, discharge voltage V_d = 45 V, Ar 1 mTorr.

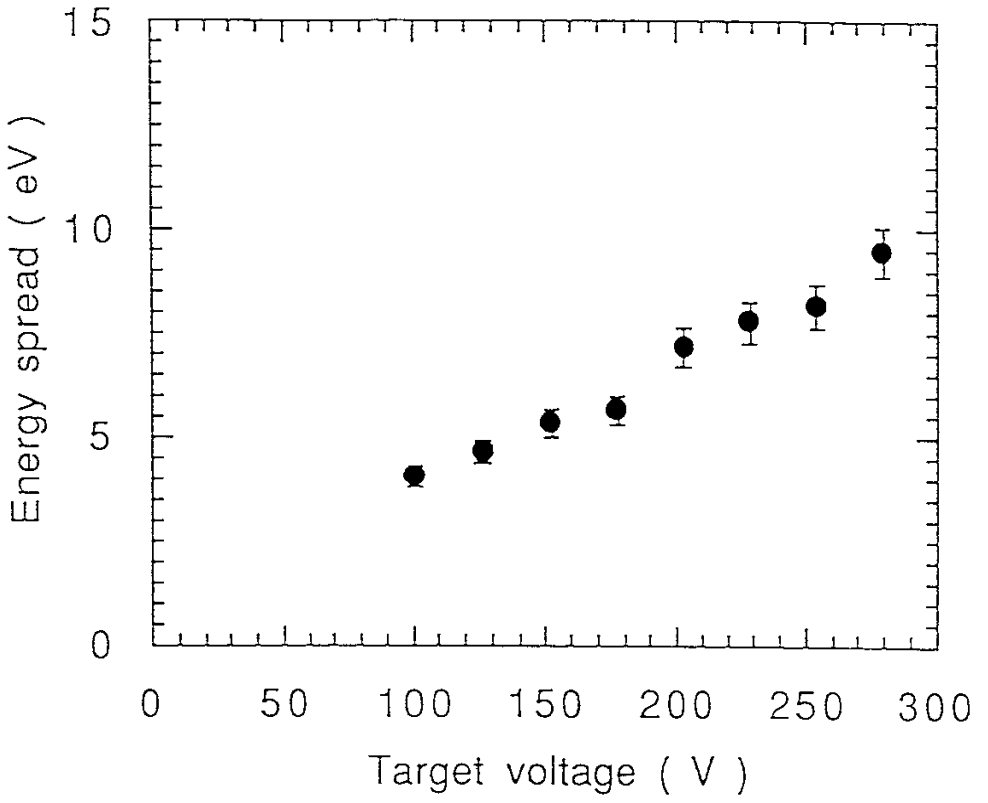

Fig. 18. The measured value of the energy spread of Au^- beam as a function of the target voltage. The experimental condition was following; discharge current I_d = 16 mA, discharge voltage V_d = 45 V, Ar 1 mTorr.

Recent Issues of NIFS Series

NIFS-54 K.Itoh and S.-I.Itoh, *Peaked-Density Profile Mode and Improved Confinement in Helical Systems*; Oct. 1990

NIFS-55 Y.Ueda, T.Enomoto and H.B.Stewart, *Chaotic Transients and Fractal Structures Governing Coupled Swing Dynamics*; Oct. 1990

NIFS-56 H.B.Stewart and Y.Ueda, *Catastrophes with Indeterminate Outcome*; Oct. 1990

NIFS-57 S.-I.Itoh, H.Maeda and Y.Miura, *Improved Modes and the Evaluation of Confinement Improvement*; Oct. 1990

NIFS-58 H.Maeda and S.-I.Itoh, *The Significance of Medium- or Small-size Devices in Fusion Research*; Oct. 1990

NIFS-59 A.Fukuyama, S.-I.Itoh, K.Itoh, K.Hamamatsu, V.S.Chan, S.C.Chiu, R.L.Miller and T.Ohkawa, *Nonresonant Current Drive by RF Helicity Injection*; Oct. 1990

NIFS-60 K.Ida, H.Yamada, H.Iguchi, S.Hidekuma, H.Sanuki, K.Yamazaki and CHS Group, *Electric Field Profile of CHS Heliotron/Torsatron Plasma with Tangential Neutral Beam Injection*; Oct. 1990

NIFS-61 T.Yabe and H.Hoshino, *Two- and Three-Dimensional Behavior of Rayleigh-Taylor and Kelvin-Helmholz Instabilities*; Oct. 1990

NIFS-62 H.B. Stewart, *Application of Fixed Point Theory to Chaotic Attractors of Forced Oscillators;* Nov. 1990

NIFS-63 K.Konn., M.Mituhashi, Yoshi H.Ichikawa,*Soliton on Thin Vortex Filament;* Dec. 1990

NIFS-64 K.Itoh, S.-I.Itoh and A.Fukuyama,*Impact of Improved Confinement on Fusion Research;* Dec. 1990

NIFS -65 A.Fukuyama, S.-I.Itoh and K. Itoh,*A Consistency Analysis on the Tokamak Reactor Plasmas;* Dec. 1990

NIFS-66 K.Itoh, H. Sanuki, S.-I. Itoh and K. Tani,*Effect of Radial Electric Field on α-Particle Loss in Tokamaks;* Dec. 1990

NIFS-67 K.Sato,and F.Miyawaki,*Effects of a Nonuniform Open Magnetic Field on the Plasma Presheath*; Jan.1991

NIFS-68 K.Itoh and S.-I.Itoh,*On Relation between Local Transport Coefficient and Global Confinement Scaling Law;* Jan. 1991

NIFS-69 T.Kato, K.Masai, T.Fujimoto,F.Koike, E.Källne, E.S.Marmar and J.E.Rice,*He-like Spectra Through Charge Exchange Processes in Tokamak Plasmas;* Jan.1991

NIFS-70 K. Ida, H. Yamada, H. Iguchi, K. Itoh and CHS Group, *Observation of Parallel Viscosity in the CHS Heliotron/Torsatron* ; Jan.1991

NIFS-71 H. Kaneko, *Spectral Analysis of the Heliotron Field with the Toroidal Harmonic Function in a Study of the Structure of Built-in Divertor* ; Jan. 1991

NIFS-72 S. -I. Itoh, H. Sanuki and K. Itoh, *Effect of Electric Field Inhomogeneities on Drift Wave Instabilities and Anomalous Transport* ; Jan. 1991

NIFS-73 Y.Nomura, Yoshi.H.Ichikawa and W.Horton, *Stabilities of Regular Motion in the Relativistic Standard Map*; Feb. 1991

NIFS-74 T.Yamagishi, *Electrostatic Drift Mode in Toroidal Plasma with Minority Energetic Particles,* Feb. 1991

NIFS-75 T.Yamagishi, *Effect of Energetic Particle Distribution on Bounce Resonance Excitation of the Ideal Ballooning Mode*, Feb. 1991

NIFS-76 T.Hayashi, A.Tadei, N.Ohyabu and T.Sato, *Suppression of Magnetic Surface Breading by Simple Extra Coils in Finite Beta Equilibrium of Helical System;* Feb. 1991

NIFS-77 N. Ohyabu, *High Temperature Divertor Plasma Operation*; Feb. 1991

NIFS-78 K.Kusano, T. Tamano and T. Sato, *Simulation Study of Toroidal Phase-Locking Mechanism in Reversed-Field Pinch Plasma*; Feb. 1991

NIFS-79 K. Nagasaki, K. Itoh and S. -I. Itoh, *Model of Divertor Biasing and Control of Scrape-off Layer and Divertor Plasmas*; Feb. 1991

NIFS-80 K. Nagasaki and K. Itoh, *Decay Process of a Magnetic Island by Forced Reconnection*; Mar. 1991

NIFS-81 K. Takahata, N. Yanagi, T. Mito, J. Yamamoto, O.Motojima and LHDDesign Group, K. Nakamoto, S. Mizukami, K. Kitamura, Y. Wachi, H. Shinohara, K. Yamamoto, M. Shibui, T. Uchida and K. Nakayama, *Design and Fabrication of Forced-Flow Coils as R&D Program for Large Helical Device*; Mar. 1991

NIFS-82 T. Aoki and T. Yabe, *Multi-dimensional Cubic Interpolation for ICF Hydrodynamics Simulation*; Apr. 1991

NIFS-83 K. Ida, S.-I. Itoh, K. Itoh, S. Hidekuma, Y. Miura, H. Kawashima, M. Mori, T. Matsuda, N. Suzuki, H. Tamai, T.Yamauchi and JFT-2M Group, *Density Peaking in the JFT-2M Tokamak Plasma with Counter Neutral Beam Injection* ; May 1991

NIFS-84 A. Iiyoshi, *Development of the Stellarator/Heliotron Research*; May 1991

NIFS-85 Y. Okabe, M. Sasao, H. Yamaoka, M. Wada and J. Fujita, *Dependence of Au^- Production upon the Target Work Function in a Plasma-Sputter-Type Negative Ion Source;* May 1991

NIFS-86 N. Nakajima and M. Okamoto, *Geometrical Effects of the Magnetic Field on the Neoclassical Flow, Current and Rotation in General Toroidal Systems*; May 1991

NIFS-87 S. -I. Itoh, K. Itoh, A. Fukuyama, Y. Miura and JFT-2M Group, *ELMy-H mode as Limit Cycle and Chaotic Oscillations in Tokamak Plasmas;* May 1991

NIFS-88 N.Matsunami and K.Kitoh, *High Resolution Spectroscopy of H^+ Energy Loss in Thin Carbon Film;* May 1991

NIFS-89 H. Sugama, N. Nakajima and M.Wakatani, *Nonlinear Behavior of Multiple-Helicity Resistive Interchange Modes near Marginally Stable States;* May 1991

NIFS-90 H. Hojo and T.Hatori, *Radial Transport Induced by Rotating RF Fields and Breakdown of Intrinsic Ambipolarity in a Magnetic Mirror*; May 1991

NIFS-91 M. Tanaka, S. Murakami, H. Takamaru and T.Sato, *Macroscale Implicit, Electromagnetic Particle Simulation of Inhomogeneous and Magnetized Plasmas in Multi-Dimensions;* May 1991

NIFS-92 S. - I. Itoh, *H-mode Physics, -Experimental Observations and Model Theories-, Lecture Notes, Spring College on Plasma Physics, May 27 - June 21 1991 at International Centre for Theoretical Physics (IAEA UNESCO) Trieste, Italy ;* Jun. 1991

NIFS-93 Y. Miura, K. Itoh, S. - I. Itoh, T. Takizuka, H. Tamai, T. Matsuda, N. Suzuki, M. Mori, H. Maeda and O. Kardaun, *Geometric Dependence of the Scaling Law on the Energy Confinement Time in H-mode Discharges;* Jun. 1991

NIFS-94 H. Sanuki, K. Itoh, K. Ida and S. - I. Itoh, *On Radial Electric Field Structure in CHS Torsatron / Heliotron;* Jun. 1991

NIFS-95 K. Itoh, H. Sanuki and S. - I. Itoh, *Influence of Fast Ion Loss on Radial Electric Field in Wendelstein VII-A Stellarator;* Jun. 1991

NIFS-96 S. - I. Itoh, K. Itoh, A. Fukuyama, *ELMy-H mode as Limit Cycle and Chaotic Oscillations in Tokamak Plasmas;* Jun. 1991

NIFS-97 K. Itoh, S. - I. Itoh, H. Sanuki, A. Fukuyama, *An H-mode-Like Bifurcation in Core Plasma of Stellarators;* Jun. 1991

NIFS-98 H. Hojo, T. Watanabe, M. Inutake, M. Ichimura and S. Miyoshi, *Axial Pressure Profile Effects on Flute Interchange Stability in the Tandem Mirror GAMMA 10;* Jun. 1991

NIFS-99 A. Usadi, A. Kageyama, K. Watanabe and T. Sato, *A Global Simulation of the Magnetosphere with a Long Tail : Southward and Northward IMF;* Jun. 1991

NIFS-100 H. Hojo, T. Ogawa and M. Kono, *Fluid Description of Ponderomotive Force Compatible with the Kinetic One in a Warm Plasma* ; July 1991

NIFS-101 H. Momota, A. Ishida, Y. Kohzaki, G. H. Miley, S. Ohi, M. Ohnishi K. Yoshikawa, K. Sato, L. C. Steinhauer, Y. Tomita and M. Tuszewski *Conceptual Design of D-^{3}He FRC Reactor "ARTEMIS"* ; July 1991

NIFS-102 N. Nakajima and M. Okamoto, *Rotations of Bulk Ions and Impurities in Non-Axisymmetric Toroidal Systems* ; July 1991

NIFS-103 A. J. Lichtenberg, K. Itoh, S. - I. Itoh and A. Fukuyama, *The Role of Stochasticity in Sawtooth Oscillation* ; Aug. 1991

NIFS-104 K. Yamazaki and T. Amano, *Plasma Transport Simulation Modeling for Helical Confinement Systems;* Aug. 1991

NIFS-105 T. Sato, T. Hayashi, K. Watanabe, R. Horiuchi, M. Tanaka, N. Sawairi and K. Kusano, *Role of Compressibility on Driven Magnetic Reconnection ;* Aug. 1991

NIFS-106 Qian Wen - Jia, Duan Yun - Bo, Wang Rong - Long and H. Narumi, *Electron Impact Excitation of Positive Ions - Partial Wave Approach in Coulomb - Eikonal Approximation* ; Sep. 1991

NIFS-107 S. Murakami and T. Sato, *Macroscale Particle Simulation of Externally Driven Magnetic Reconnection;* Sep. 1991

NIFS-108 Y. Ogawa, T. Amano, N. Nakajima, Y. Ohyabu, K. Yamazaki, S. P. Hirshman, W. I. van Rij and K. C. Shaing, *Neoclassical Transport Analysis in the Banana Regime on Large Helical Device (LHD) with the DKES Code;* Sep. 1991

NIFS-109 Y. Kondoh, *Thought Analysis on Relaxation and General Principle to Find Relaxed State;* Sep. 1991

NIFS-110 H. Yamada, K. Ida, H. Iguchi, K. Hanatani, S. Morita, O. Kaneko, H. C. Howe, S. P. Hirshman, D. K. Lee, H. Arimoto, M. Hosokawa, H. Idei, S. Kubo, K. Matsuoka, K. Nishimura, S. Okamura, Y. Takeiri, Y. Takita and C. Takahashi, *Shafranov Shift in Low-Aspect-Ratio Heliotron / Torsatron CHS* ; Sep 1991

NIFS-111 R. Horiuchi, M. Uchida and T. Sato, *Simulation Study of Stepwise Relaxation in a Spheromak Plasma ;* Oct. 1991

NIFS-112 M. Sasao, Y. Okabe, A. Fujisawa, H. Iguchi, J. Fujita, H. Yamaoka and M. Wada, *Development of Negative Heavy Ion Sources for Plasma Potential Measurement* ; Oct. 1991

NIFS-113 S. Kawata and H. Nakashima, *Tritium Content of a DT Pellet in Inertial Confinement Fusion* ; Oct. 1991

NIFS-114 M. Okamoto, N. Nakajima and H. Sugama, *Plasma Parameter Estimations for the Large Helical Device Based on the Gyro-Reduced Bohm Scaling* ; Oct. 1991